ON FURTHER MODELING OF STIFFNESS AND DAMPING OF CORRUGATED CARDBOARDS FOR VIBRATION ISOLATION APPLICATION

A Thesis

Submitted to the College of Graduate Studies and Research

in Partial Fulfillment of the Requirements

for the Degree of

Master of Science

in the

Division of Biomedical Engineering

University of Saskatchewan

Saskatoon, Saskatchewan

Canada

By

Fan Zhang

PERMISSION TO USE

In presenting this thesis in partial fulfilment of the requirements for a Master of Science degree from the University of Saskatchewan, the author agrees that the Libraries of this University may make it freely available for inspection. The author further agrees that permission for copying of this thesis in any manner, in whole or in part, for scholarly purposes may be granted by the professor or professors who supervised the thesis work or, in their absence, by the Head of the Department or the Dean of the College in which the thesis work was done. It is understood that any copying, publication, or use of this thesis or parts thereof for financial gain shall not be allowed without the author's written permission. It is also understood that due recognition shall be given to the author and to the University of Saskatchewan in any scholarly use which may be made of any material in this thesis.

Requests for permission to copy or to make other use of material in this thesis in whole or part should be addressed to:

Head of the Department of Biomedical Engineering

University of Saskatchewan

3B48 Engineering Building

57 Campus Drive

Saskatoon, Saskatchewan S7N 5A9

CANADA

ABSTRACT

In a recent study, an environment-friendly material, corrugated cardboard, was used as a building block for the vibration isolator with a preliminary study. The present thesis was motivated to advance technology for improving the design of such a corrugated cardboard vibration isolator with a focus on the modeling of its stiffness and damping.

In particular, this study has performed the following works: (1) improving the FE (finite element) model of the stiffness of the corrugated cardboards by more accurately identifying the material parameters in the cardboard material constitutive equation; (2) analyzing the effect of the error in geometry of the corrugated cardboards in the FE model; (3) developing the Rayleigh damping model of the corrugated cardboards and evaluating its accuracy.

Several conclusions were drawn from this study: (1) the parameter identification procedure based on the inverse analysis is feasible for improving the accuracy of the model of the stiffness of the cardboard. (2) The FE model of the cardboards with a greater in-plane geometrical deflection has less vertical compressive stiffness. The geometrical deflections of the corrugated cardboards also change the condition of the contact friction stress and the compressive deformation. (3) Rayleigh damping model is accurate enough for calculating the damping of the corrugated cardboards.

The contributions of the thesis include: (1) provision of a more accurate model for the compressive stiffness the corrugated cardboards, (2) finding that the friction between the cardboard and the vibrator and the geometrical error of the cardboards have a significant influence over the accuracy of the FE model, (3) finding that in practice the foregoing influence can significantly degraded the performance of the cardboards as a vibrator isolator, and (4) provision of a model for the compressive damping of the corrugated cardboards.

ACKNOWLEDGEMENTS

I would first like to thank my supervisor Professor W.J. (Chris) Zhang for his guidance, encouragement and advice. His enthusiasm and unlimited zeal on research stimulated me through my graduate study. He taught me how to think logically and how important it is to be creative and critical as a researcher. I appreciate all his contributions of time, ideas, and funding to make my master experience supportive and productive.

I am also thankful to the rest of my committee members, Professor Kushwaha, Lal and Professor Wu, Fangxiang, your valuable questions, suggestions and comments improved my work greatly. I would like to thank Jialei Huang for helping me initiate this work and sharing the relevant experiences and knowledge with me. I would like to thank Louis Roth and Douglas Bitner for the assistance of setting up experiment test-bed and offering training patiently. I would like to thank Tim May from Canadian Light Source for providing me the vacuum pump used in my experiment.

I would also like to thank my family for their support, encouragement, and unconditional love.

I also extend my gratitude to the friends in my department especially in my group. Thanks to Xu Wang, Yu Zhao, Xiaohua Hu, Tan Zhang, Bin Han, Lin Cao, Wubin Cheng, Fan Fan, Sampath Mudduda, Kirk Backstrom to discuss with me about my work. Also thanks to my friends Zhiming Zhang, Mindan Wang, Zhengshou Yang, Yu Cao for helping me settle down in Canada when I started my master study.

Finally, I would like to acknowledge the China Council Scholarship (CSC) for partly providing financial support for my master study.

DEDICATION

To my parents:

Heping Zhang and Yanqiu Li

TABLE OF CONTENTS

LIST OF FIGURES

LIST OF TABLES

LIST OF ABBREVIATIONS

AEDL	Advanced Engineering Design Laboratory
FE	Finite Element
FEM	Finite Element Method
FCT	Flat Crush Test
CMT	Concorra Medium Test
MD	Machine Direction
CD	Cross Direction
ZD	Through-thickness Direction
MPC	Multi-point Constraint
DOF	Degree of Freedom
APDL	Parametric Design Language
DV	Design variable
SV	State Variable
OV	Objective variable

CHAPTER 1 INTRODUCTION

1.1 Research Background and Motivation

Vibration of equipment in industry is usually undesirable which will make noise, reduce performance or damage equipment potentially. Motorized equipment such as pumps mounted on a solid structure or to a floor will transfer energy to the structure or to the floor in the form of vibration. Vibration isolators installed on the building structure are commonly used by engineers to reduce the harmful effect of vibration caused by the equipment. An example is shown in Figure 1.1.

Figure 1.1 Example of vibration isolators under equipment

(http://www.vibrationmountsindia.com/Vibration-Isolation-Mounts-Turret-Punch-Press.html)

Any vibration isolator is essentially a system that has stiffness and damping properties. Stiffness represents the ability of a system to resist deformation along the direction where an external force or moment is applied. Damping represents the ability of a system to dissipate the energy in the system (Rao and Horton 2003). Stiffness and damping properties are the

two most important properties of a vibration isolator. Accurate modeling of them is important to the design of the isolator.

There are various types of materials to serve as a physical body of an isolator, for example, wood, felt, rubber, paperboard, iron, etc. In our research group, Huang (2013) pioneered the study of an environment-friendly material, corrugated cardboard, for vibration isolator. In his work, the finite element (or FE) modeling of the stiffness of the cardboards was studied. Huang (2013) concluded that the FE model of the stiffness can be further improved, which was a motivation for the present thesis. Further, Huang (2013) did not include the damping in the design of the cardboard isolator, which was studied in this thesis.

1.2 Brief Review

In the past three decades, the finite element method (FEM) has been widely applied for analyzing the mechanical properties of the sandwich structures under various conditions of bending, shearing, tension, compressing and dynamic behavior. The model established with FEM was able to capture the complex property of isotropic and orthotropic materials and the contact problem. Most of the previous studies on the static stiffness property of corrugated cardboards with FEM concerned bending, buckling or shearing behavior. To the best effort of the author, only three references (Huang, 2013; Krusper et al. et al.2008; Lu et al. 2001) were found, which studied the through-thickness compressive behavior of corrugated cardboard by FEM, at least to the writer's best knowledge. However, their models did not agree well with the experimental results. In the paper of Lu et al. (2001) and Krusper et al. (2008), there is a relatively big gap between the calculated results and the experimental results. The peak of the yield point was not accurately predicted. The model of Huang (2013) improved model accuracy, with the error of 7.28% between the calculated results and the experimental results. The cause of the errors with the Huang's model may likely be the following: (1) the material parameters are not quite accurate due to the measurement limitations (Huang, 2013); and (2) the asymmetrical geometry and the frictional shear stress are presented during the compressive

process due to the plastic deformation of the material (Lu et al. 2001). In this thesis, modeling aimed at addressing the above cause was attempted.

Furthermore, the corrugated cardboards were widely used as a cushion for protecting goods from impact (Nguyen et al. 2005; Hammou et al. 2012). Further, Huang (2013) studied the characteristics of vibration isolation for corrugated cardboards subjected to the vibratory machines. Huang developed an approach to design a cardboard isolator for a vibratory machine without consideration of damping.

1.3 Research Objectives and Scope

The overall research objective of this thesis was to improve technology for designing and modeling corrugated cardboards for vibration isolation. The following specific research objectives were defined in line with this overall objective.

Objective 1: To improve the finite element model for the stiffness of corrugated cardboards in the vertical direction of vibration motion compared to the model in the paper of Huang (2013). Special attentions were paid to the constitutive equation and variable contact phenomenon.

Objective 2: To analyze how the geometric imperfection of the cardboard and the friction between the cardboard and the equipment that is on the cardboard may significantly affect the accuracy of the force-deflection relation.

Objective 3: To develop a model for the damping of the corrugated cardboards in the vertical direction of vibration motion for further improving the accuracy of the design of isolator systems composed of cardboards.

This thesis studied the characteristics of vibration in the vertical direction only and neglected the effects of the humidity and thermal influence on the cardboard from the environment.

1.4 Outline of the Thesis

This thesis includes six chapters.

Chapter 1 presents the background, motivation, a brief literature review of this study, and then proposes the objectives.

Chapter 2 gives a detailed literature review about corrugated cardboards, finite element modeling and the analysis of vibration isolator of corrugated cardboards.

Chapter 3 develops an improved finite element model of the corrugated cardboards by more accurately determining the constitutive parameters of the cardboard material. The improved model was verified by the experimental result in literature.

Chapter 4 analyzes the impact of the geometrical error of the corrugated cardboard on its stiffness modeling with the FE method.

Chapter 5 provides a Rayleigh damping model to calculate the damping of the corrugated cardboards. The accuracy of the model was verified by the experiment.

Chapter 6 concludes the thesis with the research results, the contributions and presents the future work.

CHAPTER 2 LITERATURE REVIEW

2.1 Introduction of Corrugated Cardboard

Corrugated cardboard is the most popular packaging system in industry. The corrugated cardboard is made of papers and it has the architecture as shown in Figure 2.1, which has two liners and one flute.

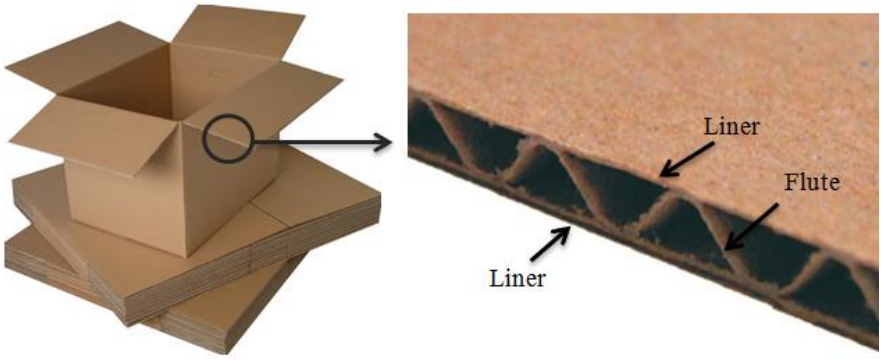

Figure 2.1 Corrugated cardboard (box and the enlarged image for an edge)

(http://www.nairaland.com/1170338/corrugated-carton-boxes)

The single-faced corrugated board (Figure 2.2) was first patented by Albert Jones who was known as 'father of the corrugated board' in 1871 in New York City (Kirwan 2012). Generally, the single–faced corrugated board was manufactured by gluing one flute with one liner. In 1874, Oliver Long improved the corrugated board to 'single-wall' (Kirwan 2012). As the most used corrugated board today, the single-wall board was produced through gluing one flute with two liners (Figure 2.2). The 'double wall' and 'triple wall' (Figure 2.2) were next to be produced to offer a higher strength to meet the variety of packaging requirements (Kirwan 2012). The major categories of the corrugated cardboards for different wall constructions are shown in Figure 2.2.

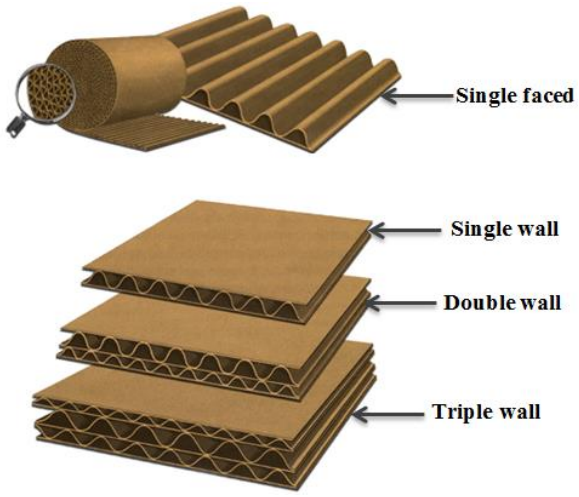

Figure 2.2 Corrugated cardboards with different wall constructions

(Twede and Selke 2005)

Corrugated cardboards can be further classified based on flute size that represents the cardboard of different strengths and performances. The different corrugated cardboards are indicated by a letter as seen in Table 2.1. In the last one hundred years of development, corrugated cardboard has changed progressively in the structure, material and manufacturing. Corrugating is one of the key steps for manufacturing the single-wall corrugated cardboard and it is schematically shown in Figure 2.3. The flutes are corrugated by rollers and then glued to liners.

Table 2.1 Specification for Corrugated Flutes (ASTM standard 2007)

Flute Designation	Flutes/m*	Flute Height (mm)
A flute	98-128	4.00-5.61
B flute	147-174	2.00-2.80
C flute	115-148	3.30-4.00
E flute	229-321	1.13-1.40

* ‘Flutes/m’ means the number of flutes per meter.

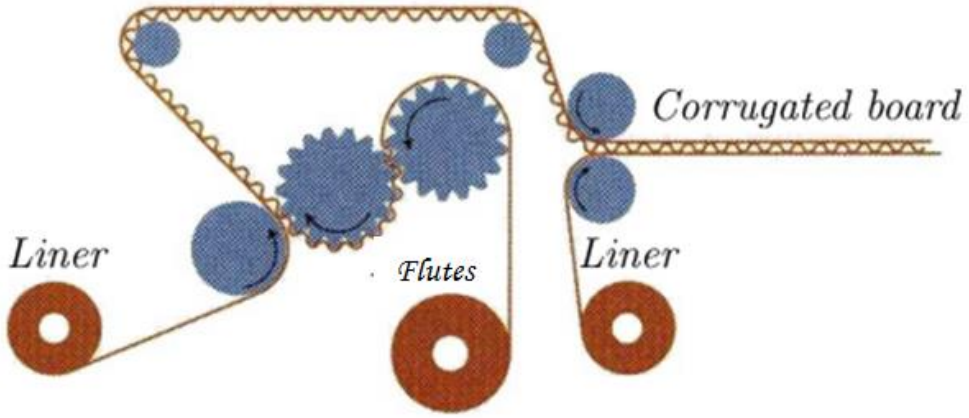

Figure 2.3 The corrugating procedure of a single wall corrugated board. (Allansson and Svärd 2001)

The manufacturing process makes fibers of the cardboards mainly oriented in the direction of the machine, which lead to the anisotropy of the cardboards (Nordstrand 2003). Cardboards are usually treated as orthotropic with three principal directions that are Machine Direction (MD), Cross Direction (CD) and through-thickness direction (ZD), as shown in Figure 2.4.

Figure 2.4 Three principal directions of the orthotropic cardboard (Nordstrand 2003)

The mechanical behaviour of corrugated cardboards can be further divided into the in-plane (x-y plane) and out-of-plane (z direction) behaviour. The in-plane and out-of-plane behaviours can be characterized by stress and strain, as shown in Table 2.2. Note that σ means stress while ε means strain, and x, y and z represent the three principal directions, respectively.

Table 2.2 Stress matrix and strain matrix

In-plane model		Out-of-plane model	
Stress	Strain	Stress	Strain
$\sigma = \begin{pmatrix} \sigma_{xx} \\ \sigma_{yy} \\ \sigma_{xy} \end{pmatrix}$	$\varepsilon = \begin{pmatrix} \varepsilon_{xx} \\ \varepsilon_{yy} \\ \varepsilon_{xy} \end{pmatrix}$	$\sigma = \begin{pmatrix} \sigma_{zz} \\ \sigma_{zx} \\ \sigma_{zy} \end{pmatrix}$	$\varepsilon = \begin{pmatrix} \varepsilon_{zz} \\ \varepsilon_{zx} \\ \varepsilon_{zy} \end{pmatrix}$

The application of corrugated cardboards ranges from the packaging and transporting products. The advantages of corrugated cardboards are eco-friendliness (completely recyclable), lightweight, low-cost and relatively high stiffness and high strength (Gilchrist et al. 1998).

2.2 Finite Element Modeling of the Corrugated Cardboard

The mean idea of Finite Element Method (FEM) is to represent a continuous structure into small but finite elements connected by their nodes. To an element, the material property and geometrical property can be manageable, leading to the governing equations for elements. The assembly of these equations leads to a system of the governing equations for the whole structure (Budynas 1999).

The previous investigations on FE analysis for the corrugated cardboards focused on different situations such as tension, compression, bending, shear, torsion, buckling and impact, and they are described briefly below.

2.2.1 Material and mechanical properties

The mechanical properties of the cardboards are determined by their raw materials. The flute component in the cardboard plays an important role in its functionality (Hammou et al. 2012). The corrugated cardboards show an anisotropic behavior in tension and compression operation. Figure 2.5 presents the typical stress-strain curves in MD, CD and the 45-degree direction in the MD and CD plane.

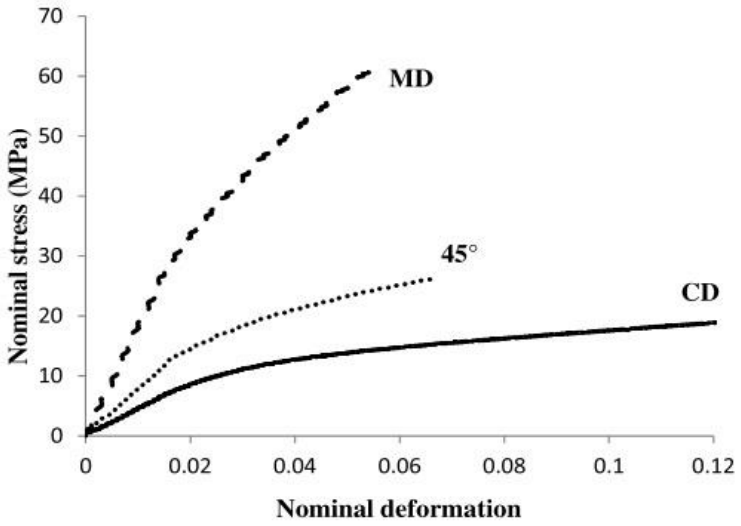

Figure 2.5 Typical strain-stress curves of corrugated cardboards under tensile test (Hammou et al. 2012)

Because the fibres in the raw material of the cardboards tend to the MD during the manufacturing process, the strength in this direction becomes quite larger than those in the other directions. The other two principal directions are CD and ZD. The corrugated cardboards are usually regarded as orthotropic in their constitutive relation.

In the previous study, some of the material parameters of corrugated cardboards were measured successfully but many others were calculated by some empirical formula. Uniaxial tension, compression and shear tests were usually applied to estimate the elastic modulus and the hardening law of the cardboards.

Baum et al. (1981) established a set of empirical formula for calculating the Poisson ratios and the in-plane shear modulus. Quite a number of papers applied Baum's formula in their models. In Baum's formula, the in-plane shear modulus is a function of in-plane young's moduli, and two out-of-plane shear moduli are proportional to the corresponding in-plane young's modulus, respectively.

In two recent works of Huang (2013) and Thakkar et al. (2008), the most commonly used method to determine the material parameters are shown in Table 2.3.

Table 2.3 The most commonly used determination method of material parameters in literature

Parameters	Meaning	Determination method
$\mathbf{E}_x$	elastic modulus in x-direction	Tensile test
$\mathbf{E}_y$	elastic modulus in y-direction	Tensile test
$\mathbf{E}_{z,}$	elastic modulus in z-direction	Empirical formula $(=\mathrm{E_x}/200)$ [1]
$\boldsymbol{\nu}_{xy,}$	Poisson ratio in xy plane	DIC [2]
$\boldsymbol{\nu}_{yz,}$	Poisson ratio in yz plane	Assumed as 0.01[3]
$\boldsymbol{\nu}_{xz,}$	Poisson ratio in xz plane	Assumed as 0.01[3]
$\boldsymbol{G}_{xy}$	Shear modulus in xy plane	Empirical formula $(=0.387\sqrt{\mathrm{E}_x\mathrm{E}_y})$[1]
$\boldsymbol{G}_{yz}$	Shear modulus in yz plane	Empirical formula $(=\mathrm{E_y}/35)$ [1]
$\boldsymbol{G}_{xz}$	Shear modulus in xz plane	Empirical formula $(=\mathrm{E_x}/55)$ [1]
$\boldsymbol{E}_t$	Tangent modulus after the yield point	Tensile test
$\boldsymbol{R}_{xx}$	yield stress ratio in x-direction	Assumed as 1
$\boldsymbol{R}_{yy}$	yield stress ratio in y-direction	Tensile test
$\boldsymbol{R}_{zz}$	yield stress ratio in z-direction	Estimate from a typical range
$\boldsymbol{R}_{xy}$	yield stress ratio in 45 °xy- plane	Estimate from a typical range
$\boldsymbol{R}_{yz}$	yield stress ratio in 45 °yz- plane	Estimate from a typical range
$\boldsymbol{R}_{xz}$	yield stress ratio in 45 °xz- plane	Estimate from a typical range

Notes: [1] Also used in the literatures (Mann et al. 1979; Baum et al. 1981; Nordstrand and Carlssonb 1997; Stenberg 2003; Aboura et al. 2004; Hammou et al. 2012)

[2] DIC: Digital Image Correlation (Thakkar et al. 2008)

[3] Also used in the literature (Nordstrand 1995)

Among the sixteen parameters, only five of them were determined by a direct measurement. The difficulty to get these constitutive parameters is seen as a bottleneck to improve the accuracy of modeling of the cardboards.

In the earlier FE analysis for corrugated cardboards, researchers usually employed the linear elastic model to model the behavior. Patel et al. (1997) created the nonlinear finite element models by following the viscoelastic constitutive law. Gilchrist et al. (1998) developed a plasticity nonlinear finite model to predict the bending and twisting behaviors. Besides the

material nonlinearity, there is nonlinearity caused from the non-linear geometry and change in the contact between components such as flute and liner.

2.2.2 Element

Beam element and shell element were the two most commonly used elements in the previous FE study for corrugated cardboards. Lu et al. (2001) and Krusper et al. (2008) adopted the beam element in their models. Lu et al. (2001) exhibited an undulating behaviour in the stress-stain curve. The model of Krusper et al. (2008) showed a smooth stress-strain curve due to the lack of nonlinear material setting, based on the author's comments. Djilali Hammou et al. (2012) used 2D shell elements to simulate both liners and the flute of the corrugated cardboard box for impact test. Haj-Ali et al. (2009) simulated the cardboard by using 3D quadratic shell finite element while Talbi et al. (2009) implemented their model into a 2D shell element in the same year. Talbi et al. (2009) also compared the 2D model with 3D model and concluded that due to the discontinuous structure of the flute along MD (x-direction), the flute's contribution to resisting compression/tension and bending in MD can be ignored and 2D theories may have sufficient accuracy; however, for certain loading conditions such as transverse shear and torsion, the 3D structure has to be considered.

2.2.3 Geometry

Carlsson et al. (2001) investigated the effect of different shapes of flute on the in-plane extensional stiffness, shear stiffness, bending stiffness and twisting stiffness. The shapes of flutes were studied included circular profile, sinusoidal profile, trapezoidal profile and triangular profile (Figure 2.6). The stiffness of cardboards with various geometry data, such as height of the cardboard and the length of flute, were also compared.

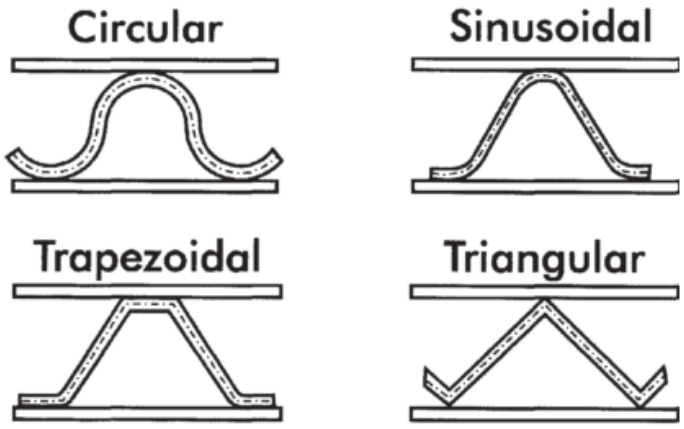

Figure 2.6 Different flute profiles in FE models (Carlsson et al. 2001)

Biancolini et al. (2003) observed that the actual flute shape is not as same as the sine shape applied in many previous FE models and obtained the cross-section contour of the actual flute by photographic magnification. Biancolini (2005) further studied the stiffness feature of saw-tooth profile, sinusoidal profile and actual profile of corrugated cardboard (Figure 2.7).

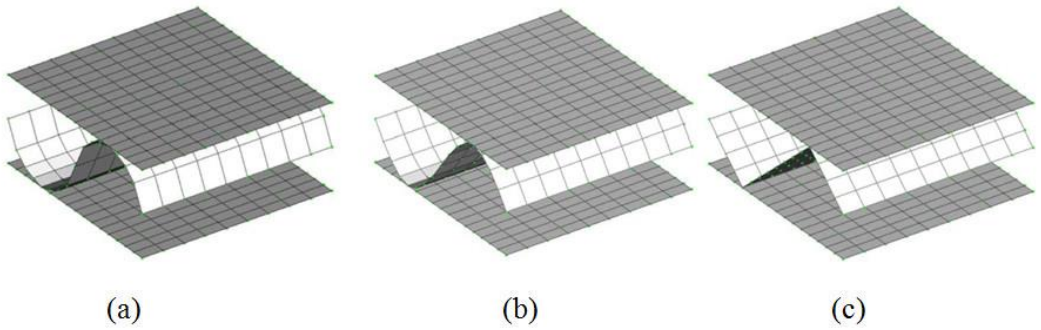

Figure 2.7 (a) Actual profile; (b) Sine profile and (c) Saw-tooth profile in FE model (Biancolini 2005)

2.2.4 Contact Problem

Adhesive: The adhesive glues flute and liners in real world and the gluing behavior may be modelled in the FE models. The assumption of fully bond was used most frequently in the previous models (Aboura et al., 2004), and this assumption further led to the model that the flute and liners shared the same nodes. Haj-Ali et al. (2009) and Jiménez-Caballero et al. (2009) utilized an isotropic and 3D solid (or called brick element) adhesive model. Pommier et al. (1991) simulated the adhesive by applying multi point constraints (MPC's) and the short shell elements, respectively. The investigations implied that the models of the adhesive

are an important factor to the stress-strain behaviour, especially the ultimate values of stress and strain (Haj-Ali et al. 2009).

Friction model: Thakkar et al. (2008), Dayyani et al. (2011) and Hammou et al. (2012) studied the friction model between flute and liners. However, to the author's best knowledge, there is little published work which studied the impact of the friction model to the performance of the whole FE model of the corrugated cardboard. In the occasion of modeling of the compression testing process, the friction between the compression head and liners is usually ignored (in particular the friction is large enough to hold together the liner and compression head); see the work of Krusper et al. et al. (2008) and Huang (2013). However, the work by Rajesh et al. (2013) observed that for a ring metal specimen rather than cardboard that the friction at the interface significantly affects its deformation and the stress-strain result under the compression test.

2.2.5 Impact and Vibration Problem

The shock or impact damage is inevitable during storage and transportation for the corrugated cardboards packages. Nguyen et al. (2005) simulated the low velocity impact of honeycomb-structure panels. By applying a software tool called Sandmesh tool for explicit impact analysis, the geometry of the indentation was predicted successfully. Sek (2009) built a FE model for multilayer corrugated cardboards structure impacted by a freefalling mass. The collapsible structure such as the corrugated cardboards exhibits the dissipative effect when subjected to impact and this effect can attenuate shock.

Djilali Hammou et al. (2012) created a homogenization FE model of free drop tests aim to deal with the impact problem of corrugated cardboards packages and claimed that the corrugated cardboards box is able to absorb shock energy. Huang (2013) confirmed the function of absorbing the dynamic energy of the corrugated cardboards and also measured the damping of cardboards, designed the cardboard-based isolator, and validated the design by experiments.

2.2.6 Compression Problem

To the best knowledge of the author, there are only three published papers, Huang (2013); Krusper et al. (2008); Lu et al. (2001) explicitly explained the FE model for the corrugated cardboards under the through- thickness- direction compression.

The FE model of Lu et al. (2001) applied the 2-D beam elements and surface contact element and behaviors by following the bi-liner constitutive law. The stress-strain curves for the specimen of two commonly used compression tests FCT (Flat Crush Test) and CMT (Concorra Medium Test) were found with FEM (Figure 2.8) (Lu et al. 2001). FCT specimen consists of the complete unit of the cardboard structure with both liner and flute while the CMT specimen has only the flute and an adhesive tape but without liners. The contact between the flute and the liners was modeled as frictionless in the simulation of FCT and as sticky in the case of CMT. The uniform compressive displacement in the through-thickness direction was applied on the upper liner of FCT model and on an imaginary rigid line where the upper liner was placed. The conclusion made was that the properties of the flute mainly drive the mechanical behavior of the corrugated cardboards subjected to a through-thickness compressive force (Lu et al. 2001).

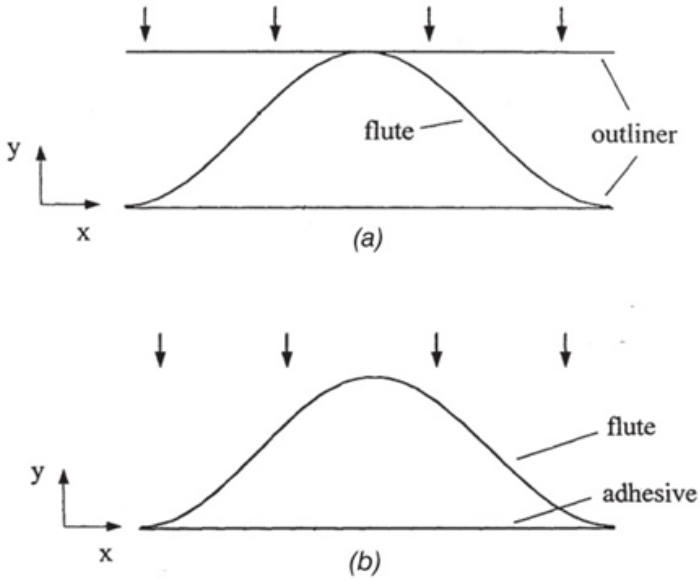

Figure 2.8 One-unit corrugated cardboards specimens for (a) FCT and (b) CMT (Lu, Chen, & Zhu, 2001)

Both of the FE models of FCT and CMT exhibited undulating curves for the stress versus strain behavior. Two different kinds of boundary conditions for the FE model were analysed in their investigation: the so-called 'periodic' boundary conditions and 'free-edge' boundary conditions. The former conditions mean that all of the DOFs of upper liner, lower liner and the flute were constrained except the vertical translations of the upper liner and the flute. The latter conditions set all of the DOFs of the liners and the flute as free but the vertical translation of the lower liner was restrained. It was reported that when the ratio of liner's thickness to flute's thickness is larger than 0.5, which is in the way of most commercially available corrugated cardboards present, the 'free-edge' boundary conditions exhibit a more accurate prediction than the 'periodic' one on the stress-strain behavior. Lu et al. (2001) also studied how the geometrical and material parameters affect the FE model's performance and the geometrical imperfection of the flute. At last, the FE results were compared with the experimental results. The comparison is shown in Figure 2.9.

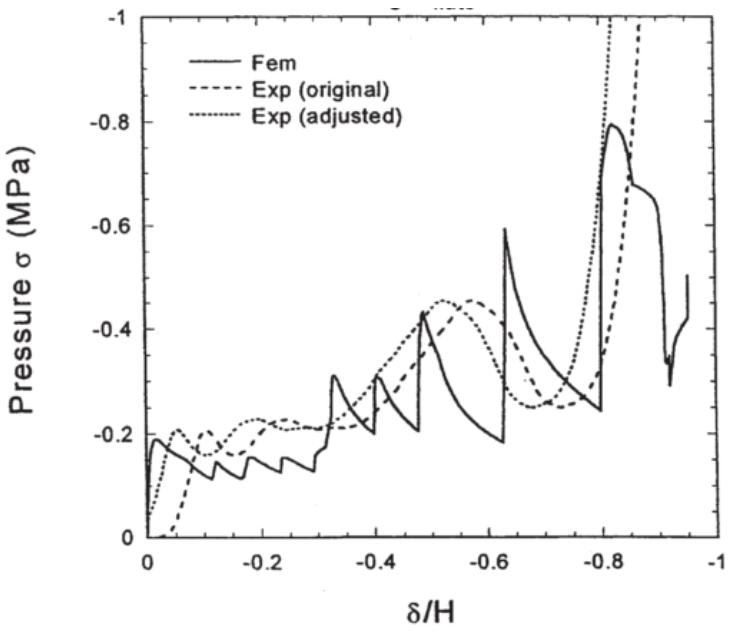

Figure 2.9 Comparison between the calculated results and the experimental results (Lu et al. 2001)

It can be seen from the comparison plot that the predicted compressive responses do not coincide with those measured well, both in linear portion and in nonlinear portion. The author explained by the following reasons:

1. Since no geometrical deviation in the finite element mesh for the fluting, the calculated deformation pattern is symmetrical throughout; hence, the panel hardens and softens significantly and sharply.

2. The predicted initial stiffness is larger than that measured, and the calculated stress versus strain curve shows more wiggles than the measured curve dose , which may attributed to the higher sensitivity of the finite element simulation to localized collapse of the fluting than that of the test machine.

There is another possible reason: the constitutive parameters relative to nonlinear properties may be not proper. That can be preliminary verified by changing the constitutive parameters properly in the finite element model, the stress versus strain curve may approach to the measured curve considerably.

Krusper et al. (2008) developed an analytical model for calculation the nonlinear deformation of the fluting under vertical compressive loads and compared the analytical model with a finite element model and with experimental results. The comparison is shown in Figure 2.10 where the FE results agree well with the analytical results. In particular, the linear part in the experimental curve agrees well with those in both analytical and FE model curve. However, there is a big difference in the nonlinear part. This is because the nonlinear material properties of the flute and the liner in the FE model were not considered.

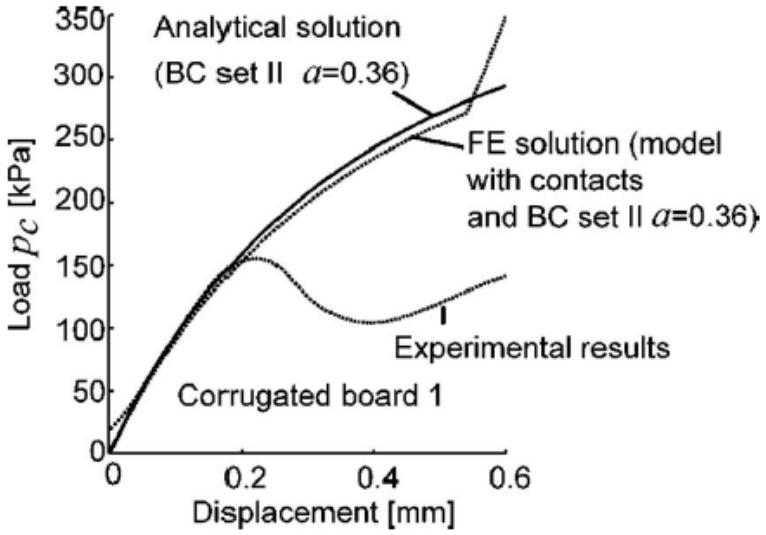

Figure 2.10 Comparison between solutions obtained by analytic model, FE model and experiment (Krusper et al., 2008)

Huang (2013) refined the finite element model of Lu et al. (2001) and Krusper et al. (2008) by changing the element type from beam element to the shell element and by considering the nonlinear orthotropic material property. The constitutive model in Huang's work consisted of two parts: the elastic portion and the plastic portion. The elastic portion followed the Hook's Law, while the plastic part was governed by a quadratic Hill yield criterion. In these constitutive models, there were sixteen unknown parameters in total, but only four of them were experimentally measured, while the other value of parameters were derived by the empirical formula or from an empirical range (see details in Table 2.3). The comparison between the FEM results and the experimental results (60.8 mm×38 mm) is shown in Figure 2.11. It can be found from the figure that the FEM result dose not correlate well with the

experimental result in the nonlinear portion (after reaching the peak at the displacement of about 0.75 mm). This situation is because the plastic model property was not correct.

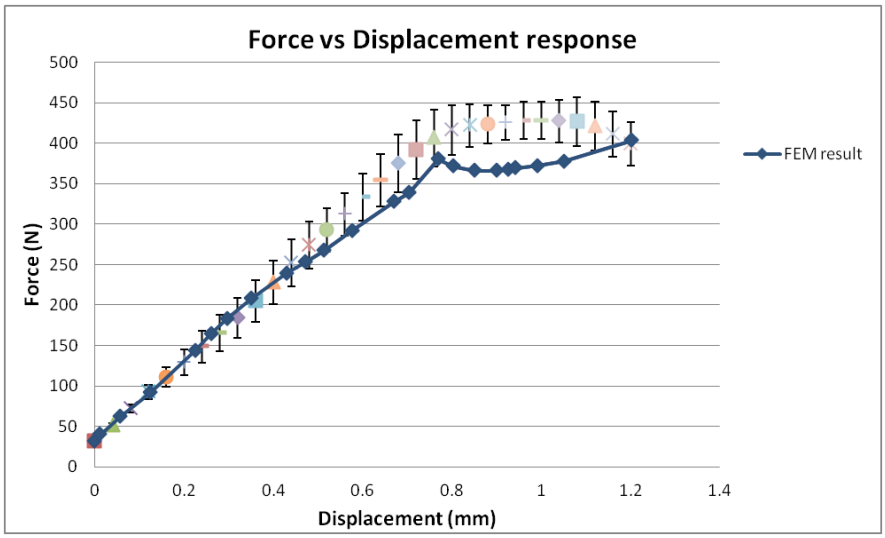

Figure 2.11 Comparison of the experimental results and FEM results (Huang 2013)

Overall, Lu et al. (2001), Krusper et al. (2008) and Huang (2013) performed a finite element analysis for the cardboard by considering some non-linear behavior of the cardboard. However, there is a common disadvantage in their models: the peak load and the subsequent nonlinear response cannot be predicted accurately. This is because the nonlinear material property of the cardboard in their models is not accurate.

2.3 Vibration Isolation

Vibration isolations are divided into two categories: passive isolation and active isolation. Passive vibration isolation refers to vibration isolation methods of using the materials such as rubber pads, mechanical springs or sheets of flexible materials. Active vibration isolation refers to employing the electric power, sensors, actuators, and control systems to adjust the isolation behavior in a real-time fashion (De Silva 2006). The mean advantage of the passive system over the active system is that the passive system is less expensive and easy to construct. The corrugated cardboard, which is used as vibration isolation in this study, is considered as a passive isolation system.

The principle of vibration isolation is illustrated by a single-degree of freedom vibration system, as shown in Figure 2.12. The equipment is considered as a rigid body subjected to the vertical vibration force only and the isolator is placed between the equipment and ground. The isolation system consists of the mass element (inertia), spring element (stiffness), and damping element (damping).

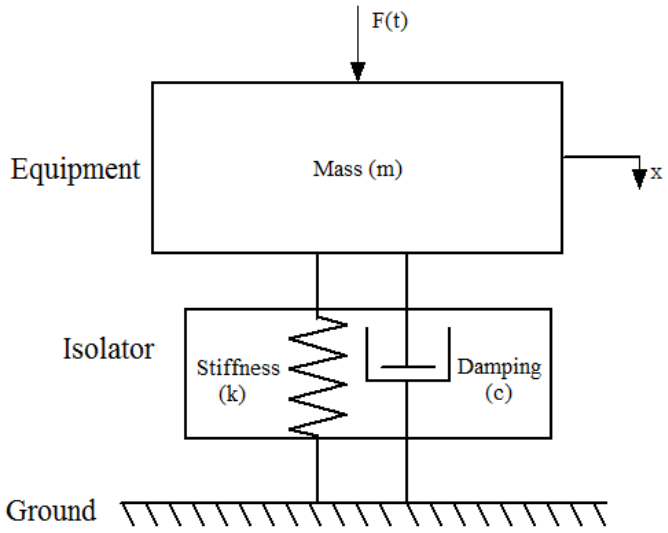

Figure 2.12 The schematic diagram for a Single-degree of freedom vibration system

The spring element refers to any elastic element. In the one single-degree of freedom vibration system, the spring is assumed to be massless and linear. In addition to the most familiar coil spring, the general mechanical system involving elastic element involves the elastic deformations of many other structures such as beams and robs. Stiffness is one of the essential features of the spring element of a vibration isolation system.

Damping is defined as the energy dissipation that causes vibration energy converted to other kinds of energy such as heat energy or mechanical energy. Damping can be classified into two categories: the inherent material damping and the other kinds of energy dissipation such as friction at joints. In the composite structure, without many joints to cause frictional energy dissipation, the inherent material damping often dominates the overall vibration behavior. Damping of a system mainly depends on the material, velocity of motion, and frequency of vibration. Huang (2013) developed an approach to design the cardboard isolator for a

vibratory machine. However, the damping was ignored in his approach, which may need more deliberation and re-thinking.

2.4 Conclusion

This chapter introduced the background and reviewed the literature about corrugated cardboards with a focus on its application of vibration isolation and the finite element modeling. The discussion may have given a sufficient argument that the accuracy of the FE model may be improved by giving further attention to the determination of the material parameters in the constitutive relation. Further, more accurately modeling the contact between the liner and flute in the cardboards may also be a factor to improve the accuracy of the model. Last, the damping behavior may need to be studied in the context of the vibration isolation system made of the cardboards.

CHAPTER 3 DETERMINATION OF CONSTITUTIVE PARAMETERS

3.1 FE Model

The FE model of the corrugated cardboards in this paper was built upon the model of Huang (2013). In the following, this model is explained.

3.1.1 Element

Shell elements were used to analyze the thin structures. In this case, the shell 181 was used due to its better performance to deal with the nonlinearity. The shell 181 element is a first-order quadrilateral element. It is defined by four nodes: I, J, K, L with three translational and three rotational degrees of freedom at each node, as seen in Figure 3.1. Figure 3.1 also denotes the geometry, node locations, and the element coordinate system for this element. Note x and y are in the plane of the element. The default orientation of the element coordinate system is $\theta = 0$ (Figure 3.1).

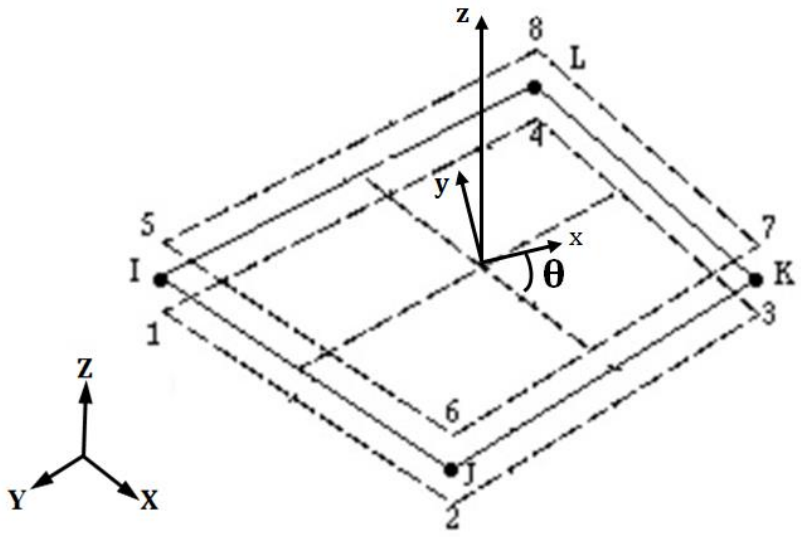

Figure 3.1 The geometry of the shell 181 element(ANSYS Inc. 2004)

The shell 181 element obeys the Mindlin theory which has basic assumptions (Imaoka 2000; ANSYS Inc. 2004). (1) The straight line normal to the mid-surface before deformation remains straight after loading, but not necessarily normal to the mid-surface. (2) The through-thickness stress is negligible. (3) Each set of integration points thru a layer is assumed to have the same element (material) orientation. (4) The change in thickness is due to the "stretching" of the shell only. It is noted that the major advantage of shell 181 is that it is capable of large deformation and it supports most material nonlinearities.

3.1.2 Nonlinearity

In the finite element analysis process, the nonlinear problems fall into the following three categories, and all of them are considered in this study. The three kinds of nonlinear behaviors or properties of the material are (1) Geometrical nonlinearity (2) material nonlinearity, and (3) boundary condition nonlinearity.

Geometry nonlinearity is caused by large deformation of the element such that the relationship between load and deformation is not linear. For instance, the so-called continuity equation is not linear; in particular the relationship between the strain and displacement and its derivative is not linear. Material nonlinearity refers to the material constitutive relation in particular the stress and strain relationship is nonlinear. Boundary condition nonlinearity refers to the relationship between force and displacement and its derivative on the boundary is nonlinear. A typical problem of boundary nonlinearity comes from the contact problem.

3.1.3 Contact problems

In this model, the liner and the core share the same node and apply to the surface-to-surface contact condition in their connecting area. In the surface-to-surface contact condition, it is important to identify contact surface and target surface since the contact algorithm set rules that the nodes on the target surface cannot penetrate into the contact surface. There are several intuitive but rough criterions commonly used to select the contact surface and target surface, such as the convex, softer, smaller; otherwise fine meshed surfaces are usually selected as the contact surface while the concave, flat, coarse meshed, stiffer or lager surfaces

are usually considered as the target surface. In this study, the contact surface is assigned to the surface of the flute and the target surface is set to the surface of the liner.

3.2 Constitutive law

As mentioned above, Huang's constitutive model consists of the elastic portion following the Hook's Law and the plastic portion governed by Hill yield criterion and isotropic hardening law. The elastic orthotropic constitutive model is assumed to be one as follows (Allansson and Svärd 2001):

$$\begin{bmatrix} \varepsilon_x \\ \varepsilon_y \\ \varepsilon_z \\ \gamma_x \\ \gamma_y \\ \gamma_z \\ \end{bmatrix} = \begin{bmatrix} \frac{1}{E_x} & \frac{-\nu_{yx}}{E_y} & \frac{-\nu_{zx}}{E_z} & 0 & 0 & 0 \\ \frac{-\nu_{xy}}{E_x} & \frac{1}{E_y} & \frac{-\nu_{zy}}{E_z} & 0 & 0 & 0 \\ \frac{-\nu_{xz}}{E_x} & \frac{-\nu_{yz}}{E_y} & \frac{1}{E_z} & 0 & 0 & 0 \\ 0 & 0 & 0 & \frac{1}{G_{xy}} & 0 & 0 \\ 0 & 0 & 0 & 0 & \frac{1}{G_{xz}} & 0 \\ 0 & 0 & 0 & 0 & 0 & \frac{1}{G_{yz}} \end{bmatrix} \times \begin{bmatrix} \sigma_x \\ \sigma_y \\ \sigma_z \\ \tau_{xy} \\ \tau_{xz} \\ \tau_{yz} \end{bmatrix} \tag{3.1}$$

where

$\varepsilon_x, \varepsilon_y, \varepsilon_z$: strain in x, y, z direction,

γ_{xy}, γ_{xz}, γ_{yz} : strain in xy, xz, yz plane,

E_x, E_y, E_z : Young's modulus in x, y, z direction,

ν_{xy}, ν_{xz}, ν_{yz} : Poisson's ratio in xy, xz, yz plane, and

G_{xy}, G_{xz}, G_{yz} : shear modulus in xy, xz, yz plane.

The yield criterion is given by (ANSYS Inc. 2004)

$$f\{\sigma\} = \sqrt{\{\sigma\}^T [M] \{\sigma\}} - \sigma_0(\varepsilon^p) = 0 \tag{3.2}$$

where

σ_0 : yield stress in the x direction,

ε_P : equivalent plastic strain,

$\{\sigma\}$: yield stress matrix, and

$[M]$: plastic compliance matrix.

The plastic compliance matrix $[M]$ (ANSYS Inc. 2004) can be written as:

$$[M]=\begin{bmatrix} G+H & -H & -G & 0 & 0 & 0 \\ -H & F+H & -F & 0 & 0 & 0 \\ -G & -F & F+G & 0 & 0 & 0 \\ 0 & 0 & 0 & 2K & 0 & 0 \\ 0 & 0 & 0 & 0 & 2I & 0 \\ 0 & 0 & 0 & 0 & 0 & 2J \end{bmatrix} \tag{3.3}$$

F, G, H, I, J and K are material constants that can be determined experimentally. According to ANSYS (2004), these are defined as:

$$F=\frac{1}{2}\left(\frac{1}{R_{yy}^2}+\frac{1}{R_{zz}^2}-\frac{1}{R_{xx}^2}\right) \tag{3.4}$$

$$G=\frac{1}{2}\left(\frac{1}{R_{zz}^2}+\frac{1}{R_{xx}^2}-\frac{1}{R_{yy}^2}\right) \tag{3.5}$$

$$H=\frac{1}{2}\left(\frac{1}{R_{xx}^2}+\frac{1}{R_{yy}^2}-\frac{1}{R_{zz}^2}\right) \tag{3.6}$$

$$I=\frac{3}{2}\left(\frac{1}{R_{yz}^2}\right) \tag{3.7}$$

$$J=\frac{3}{2}\left(\frac{1}{R_{xz}^2}\right) \tag{3.8}$$

$$K = \frac{3}{2}\left(\frac{1}{R_{xy}^2}\right) \tag{3.9}$$

In the above, the ratios of yield stresses $R_{xx}, R_{yy}, R_{zz}, R_{xy}, R_{yz}$ and R_{xz} (ANSYS Inc. 2004) are further calculated by

$$R_{xx} = \frac{\sigma_{xx}^{y}}{\sigma_0} \tag{3.10}$$

$$R_{yy} = \frac{\sigma_{yy}^{y}}{\sigma_0} \tag{3.11}$$

$$R_{zz} = \frac{\sigma_{zz}^{y}}{\sigma_0} \tag{3.12}$$

$$R_{xy} = \sqrt{3}\frac{\sigma_{xy}^{y}}{\sigma_0} \tag{3.13}$$

$$R_{yz} = \sqrt{3}\frac{\sigma_{yz}^{y}}{\sigma_0} \tag{3.14}$$

$$R_{xz} = \sqrt{3}\frac{\sigma_{xz}^{y}}{\sigma_0} \tag{3.15}$$

where σ_{ij}^{y} is the yield stress in the x, y, z, xy, yz and xz directions, respectively. The six yield stress ratios are direct input items in the FE model when the reference stress σ_0 is defined – see Equation (3.10) to (3.15).

The hardening rule determines when the material will yield again if the loading is continued or reversed. There are two basic hardening rules to prescribe the evolution of the yield surface compared to the Initial Yield surface: Kinematic hardening and Isotropic hardening. Isotropic hardening means that the yield surface remains constant in size and translates in the direction of yielding. The Isotropic hardening implies that the yield surface increases in size uniformly in all directions with the plastic flow. For a solid that follows the isotropic

hardening rule, if it is unloaded after a plastic deformation, reloading it again will lead to its yield stress to increase. The isotropic hardening rule is chosen to describe such plasticity.

Therefore, the plastic slope of the material after yield point (ANSYS Inc. 2004) is:

$$E^{pl} = \frac{E_x E_t}{E_x - E_t} \tag{3.16}$$

where

E_x : Elastic modulus in x direction, and

E_t : Tangent modulus after the yield point.

There are sixteen parameters in the constitutive law of the cardboard in this case and these are $E_x, E_y, E_z, \nu_{xy}, \nu_{yz}, \nu_{xz}, G_{xy}, G_{yz}, G_{xz}$ and E_t, $R_{xx}, R_{yy}, R_{zz}, R_{xy}, R_{yz}$ and R_{xz}. These parameters and their physical meanings are explained in Table 3.1 (Huang 2013).

Table 3.1The parameters in the constitutive law of the model of the cardboard

Parameters	Meaning
$\mathbf{E_x}$	Elastic modulus in x-direction
$\mathbf{E_y}$	Elastic modulus in y-direction
$\mathbf{E_z}$,	Elastic modulus in z-direction
$\boldsymbol{\nu_{xy}}$,	Poisson ratio in xy plane
$\boldsymbol{\nu_{yz}}$,	Poisson ratio in yz plane
$\boldsymbol{\nu_{xz}}$,	Poisson ratio in xz plane
$\boldsymbol{G_{xy}}$	Shear modulus in xy plane
$\boldsymbol{G_{yz}}$	Shear modulus in yz plane
$\boldsymbol{G_{xz}}$	Shear modulus in xz plane
$\boldsymbol{E_t}$	Tangent modulus after the yield point
$\boldsymbol{R_{xx}}$	Yield stress ratio in x-direction
$\boldsymbol{R_{yy}}$	Yield stress ratio in y-direction
$\boldsymbol{R_{zz}}$	Yield stress ratio in z-direction
$\boldsymbol{R_{xy}}$	Yield stress ratio in 45 °xy- plane
$\boldsymbol{R_{yz}}$	Yield stress ratio in 45 °yz- plane
$\boldsymbol{R_{xz}}$	Yield stress ratio in 45 °xz- plane

The necessity to conduct the identification for each parameter in the constitutive function of the cardboard-model will be analyzed and the selected parameters will be identified through the numerical-experimental identification procedure.

3.3 Experimental Setup

To determine the aforementioned constitutive parameters, a system for the measurement of the behaviour of corrugated cardboards needs to be set up. The behavior considered in this study was the stiffness in the vertical direction or ZD (Figure 2.4). In this case, the setup used for building Huang's FE model was used. Further, the commercially available corrugated cardboard from the Company denoted as C was used in the compression (along ZD) experiment. The geometry for the type-C cardboard is shown in Figure 3.2 and the geometrical parameters of the cardboard are listed in Table 3.2.

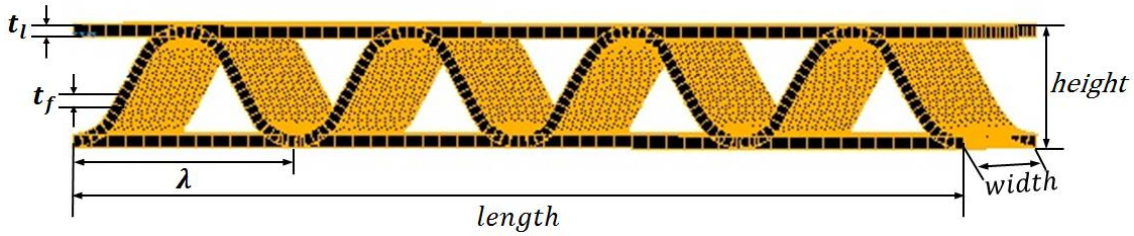

Figure 3.2 Geometry of the type-C cardboard

Table 3.2 Geometry of the corrugated cardboard specimen (mm)

Flute Type	Length	Width	Height	Flute length (λ)	Thickness of liner (t_l)	Thickness of flute (t_f)
C	30.4	38	3.6	7.6	0.28	0.28

The through-thickness compressive test for the corrugated cardboards followed the method in the thesis of Huang (2013). The force verses displacement curve was recorded through the compressive test. Figure 3.3 depicts a typical force-displacement curve drawn from the compressive test. Due to the so-called 'washboard effect' (i.e., the non-flatness of the liner), the initial stage of a force-displacement curve of the experimental result was neglected.

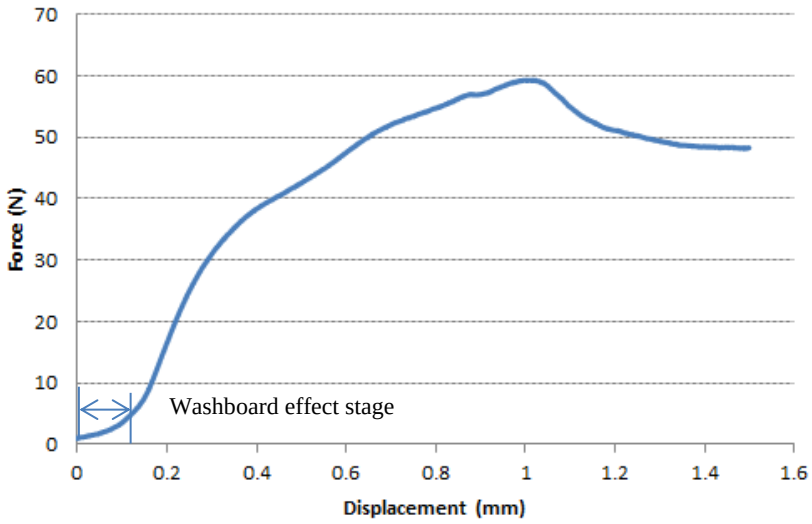

Figure 3.3 The typical force-displacement curve in compressive experiment

3.4 Parameter identification procedure

The general idea of application of the system identification technique to the determination of the system parameter was to determine the parameter in a system or model based on the fitting of the behavior of the system predicted and measured on a particular instance. In our case, the parameter is the constitutive parameter of the cardboard, and the behavior is the stiffness along ZD, and the prediction method is the finite element method (as described in the above). In applying this technique, the parameters in a model are thus taken as a variable and the problem model is an optimization problem.

The commercial software ANSYS® with the built-in OPT processor was adopted as an optimization tool. ANSYS allows the user to choose the optimization algorithm and to define the objective function, design variables and constraints (ANSYS Inc. 2005). Three steps were followed to accomplish this task: (1) Define design variables (DVs), (2) Define State Variables (also called constraint, SVs), and (3) Define objective variables (OVs).

3.4.1 Design variables (DVs)

Design variables are those 16 constitutive parameters (see Table 3.1). Because the liner and flute have the same constitutive equation but different constitutive parameters, there are in total 32 parameters. To an optimization problem, 32 parameters may create some

computational overhead. It is certainly helpful to reduce the number of variables in optimization. Therefore, an attempt to discard some parameters was taken. A general principle to get rid of some parameters is to examine the significance of their effect of the parameters on the response of the FEM model, that is, force-displacement curve in this case. A coefficient R was introduced to represent the sensitivity of the parameters to the force-displacement curve, which is the ratio of the percent change of the ultimate force in the force-displacement curve and the change in the material parameters.

$$R = \frac{\Delta \text{ ultimate force } \%}{\Delta \text{material parameter } \%} \tag{3.17}$$

Another principle is to examine the effects of the parameters in terms of their physical meanings, and for this purpose, the 32 parameters are divided into five groups that have the physical meaning.

a. Young's modulus

Following the assumption in the shell 181 element, the stress through-thickness is considered as zero (ANSYS Inc. 2005). This further implies that any change in the thickness of the element is due to the "stretching" of the shell only and the thickness of the element will not change when the element is compressed along the thickness direction. Thus, $E_z \equiv 0$, where E_z is the out-of-plane young's modulus (see Figure 3.1).

$E_z$will not affect the result of the finite element calculation for the shell element. This was verified by the calculation with the FEM for different E_z (in particular by randomly changing E_z of either flute or liner material or both). The calculation showed no significant change against a reference force-displacement curve. In fact, this can also be explained by Mindlin's theory of plates that there is no through-thickness stress in plates; therefore, the young's modulus in z-direction would be considered as zero.

For the in-plane Young's modulus (i.e., E_{xl}, E_{xf}, E_{yl} and E_{yf}), these were changed incrementally (see Table 3.3) and then calculate the stiffness along the z-direction for the

different increments of them. It is noted that in the term of E_{xl}, E_{xf}, E_{yl} and E_{yf}, *x* and *y* refer to the two axes as denoted in Figure 3.1, and further, 'l' means liner and 'f' means the flute. For example, E_{xl} means the elastic modulus in the x-direction for the liner. In total, nine models were created by changing one Young's modulus each time by using model 1 as the reference model. Unless otherwise stated in this chapter, model 1, also called the reference model, is the same as that in Huang's thesis (Huang 2013).

After calculations, the force-displacement curves of the nine models are obtained. The ultimate forces of the nine force-displacement curves are listed in Table 3.3.

Table 3.3 Sensitivity of In-plane Young's moduli in comparison calculations

Model number	1 (Reference)	2	3	4	5	6	7	8	9
Changed parameter	———	E_{xl}	E_{xl}	E_{xf}	E_{xf}	E_{yl}	E_{yl}	E_{yf}	E_{yf}
Changed value (Gpa) (Reference value)	———	2.5 (3.2)	5.0 (3.2)	2.5 (3.2)	5.0 (3.2)	1 (2)	3 (2)	1 (2)	3 (2)
Ultimate force (N)	197.69	197.69	197.69	195.27	202.09	197.69	197.69	197.70	197.86
Sensitivity R	———	0	0	3.46	2.44	0	0	-0.01	0.17

The calculated results showed that the in-plain Young's moduli of liner E_{xl} (model 1, 2 and 3) and E_{yl} (model 1, 6 and 7) had no influence on the stress-strain response with a sensitivity of zero. The calculated result showed a strong independence on E_{yf} (model 1, 8 and 9) by an average sensitivity of 0.08 for increase and decrease. E_{xf} (model 1, 4 and 5) affects the stress-strain curve more strongly with an average sensitivity of 2.95. In conclusion, the six design parameters of Young's moduli reduce to only one key parameter E_{xf} which has a significant influence.

b. Poisson's ratios

Poisson's ratios are classified into two categories based on the directions. These are in-plane Poisson's ratio ν_{xy} and the out-of-plane Poisson's ratios ν_{yz} and ν_{xz}. The in-plane Poisson's ratio is measured by tensile test as the form of a ratio of lateral to longitudinal strain. The out-of-plane Poisson's ratios are generally neglected in literatures due to its relatively small effect to the compression response. In the papers of Thakkar et al. (2008) and Huang (2013), $\nu_{yz,}\nu_{xz}$ are assumed to be 0.01. To verify whether the Poisson's ratios have any effect on the compression response, ten calculations were taken. First four calculations changed ν_{xy} from 0.3 to 0.45 with an interval of 0.05 and six other one assigned 0.01, 0.05 and 0.1 to ν_{yz} and ν_{xz} separately. Only one parameter was changed in each calculation, while all the rest parameters stayed the same as these were in the reference model. The force-displacement results show that there is barely change in these calculations, which imply that change of the Poisson's ratios $\nu_{xy}, \nu_{yz}\, and\, \nu_{xz}$ has negligible influence on the calculated result in this FE model. Note that the results in this section are applicable to Poisson's ratios of both the flute and liner.

c. Shear modulus

The shear moduli were often calculated with empirical formulas (Mann et al. 1979; Baum et al. 1981) in literature. To examine whether the shear moduli affect the response of the compression model, the calculations were taken. The values of the changed parameters and their reference values are listed in Table 3.4. Model 1 is the reference model. Models 2-7 reduced each shear modulus by half while all the rest parameters keep the same as these are in the reference model. The force-displacement characteristics under these conditions are plotted in Figure 3.4.

Table 3.4 Sensitivity of Shear moduli in comparison calculations

Model Number	1 (Reference)	2	3	4	5	6	7
Changed parameter	——	G_{xyl}*	G_{xyf}*	G_{xzl}	G_{xzf}	G_{yzl}	G_{yzf}
Changed value (GPa) (Reference value)	——	0.5 (1)	0.5 (1)	0.057 (0.0285)	0.005 (0.0025)	0.058 (0.029)	0.05 (0.025)
Ultimate force (N)	197.69	197.69	197.69	197.69	122.60	197.69	197.71
Sensitivity R	——	0	0	0	-3e4	0	-0.8

* G_{xyl} means the shear modulus of liner in xy-plane; G_{xyf} is the shear modulus of flute in xy-plane, etc.

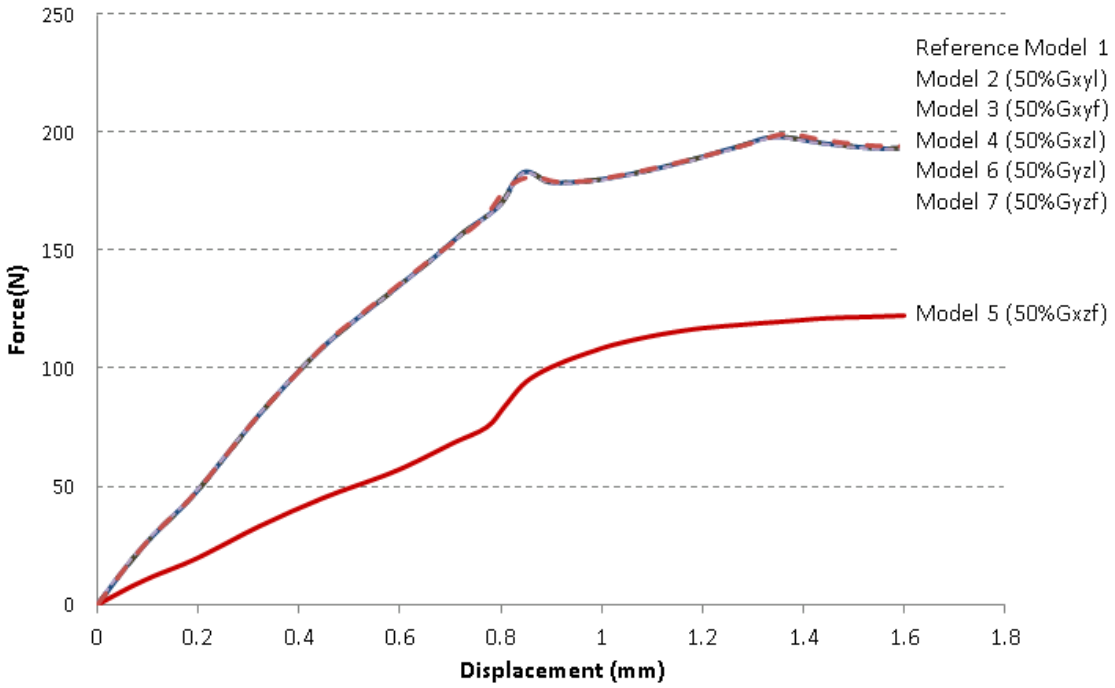

Figure 3.4 The force-displacement curves with different Shear moduli

The force-displacement curves of the model 1-7 shows that none of the shear moduli affects the result of the calculation significantly except the model 5 (related to G_{xzf}). It can be found in Table 3.4 that the response of the model 5 strongly depends on G_{xzf} with the sensitivity of

-3e4. Figure 3.4 shows that G_{xzf} has a great influence on both the elastic portion and the plastic portion in the force-displacement curve. It is noted that the strong influence of the out-of-plane shear moduli on the frequency property rather than the stiffness property of paperboards was verified in the previous study by Schwingshackl et al. (2006). The analysis here seems to be in consistence with their result.

d. Tangent modulus

Tangent modulus of liner E_{tl} was changed from 2.5GPa in the reference model to be 0.01GPa, 1.25GPa and 0.25GPa, where Tangent modulus of flute E_{tf} was also set in the reference model 0.01GPa, 0.005GPa, and 0.001GPa (Table 3.5). Other parameters were set up the same as that in the reference model. Table 3.5 shows the sensitivity of Tangent moduli. The force-displacement results of the FE model with different Tangent moduli are shown in Figure 3.5.

Table 3.5 Sensitivity of Tangent moduli in comparison calculations

Model number	1 (Reference)	2	3	4	5
Changed parameter	——	E_{tl}	E_{tl}	E_{tf}	E_{tf}
Changed value (GPa) (Reference value)	——	1.25 (2.5)	0.25 (2.5)	0.005 (0.01)	0.001 (0.01)
Ultimate force (N)	197.69	197.69	197.69	202.29	205.17
Sensitivity R	——	0	0	-9.2e2	-8.3e2
Average sensitivity	——	0		-8.8e2	

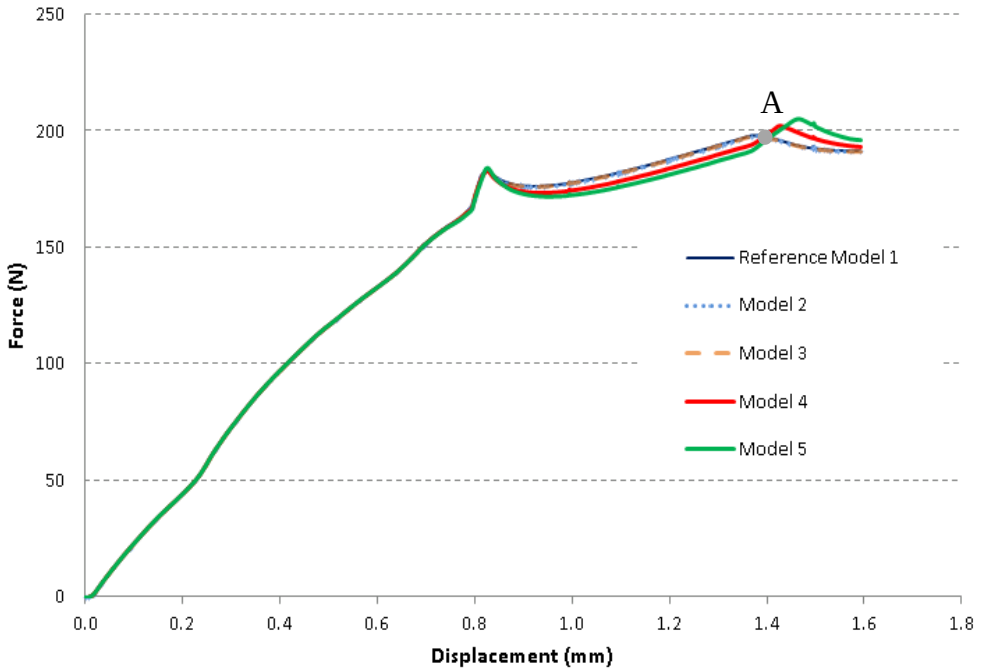

Figure 3.5 The force-displacement curves with different tangent moduli

From Table 3.5 and Figure 3.5, it can be seen that E_{tl} has no influence on the response and with the model 1, 2 and 3, while E_{tf} has more significant influence on the response curve with the model 1, 4 and 5. Note that the influence only presents in the plastic portion. Moreover, E_{tf} have a positive correlation with the force from the yield point to the point A and a negative correlation after the point A (Figure 3.5). The average of the sensitivity to the ultimate force is -8.8e2 (Table 3.5).

e. Yield stress ratios

There are six parameters characterizing the Hill yield criterion in the FE model, which are yield stress ratios $R_{xx}, R_{yy}, R_{zz}, R_{xy}, R_{yz}$ *and* R_{xz} (ANSYS Inc. 2004) (see Chapter 1 for details). The analysis showed that only the yield stress ratio in the x-direction R_{xx} has a significant influence on the force-displacement curve while the other five ratios make no difference and can thus be neglected. Table 3.4 lists the sensitivity of R_{xx} in the range of 0.5 to1. From this table, it can be seen that R_{xx} strongly affects the force-displacement curves with the average sensitivity of 88.62. The response curves with a different R_{xx} are plotted in Figure 3.6. It can be seen from the figure that R_{xx} strongly affects the plastic behavior of the

model. All of the curves in Figure 3.6 with R_{xx} from 0.5 to 1 start to split after reaching their common proportional limit (point 'P' in Figure 3.6). It can also be found that the yield strength of the cardboard increases with the increase of R_{xx}.

Table 3.6 Sensitivity of R_{xx} in comparison calculations

Model Number	1 (Reference)	2	3	4	5	6
Changed value	1	0.9	0.8	0.7	0.6	0.5
Ultimate Force (N)	197.69	188.11	181.32	172.11	161.06	150.99
Sensitivity R	——	95.8	81.85	85.27	91.58	93.4
Average Sensitivity	——	88.62				

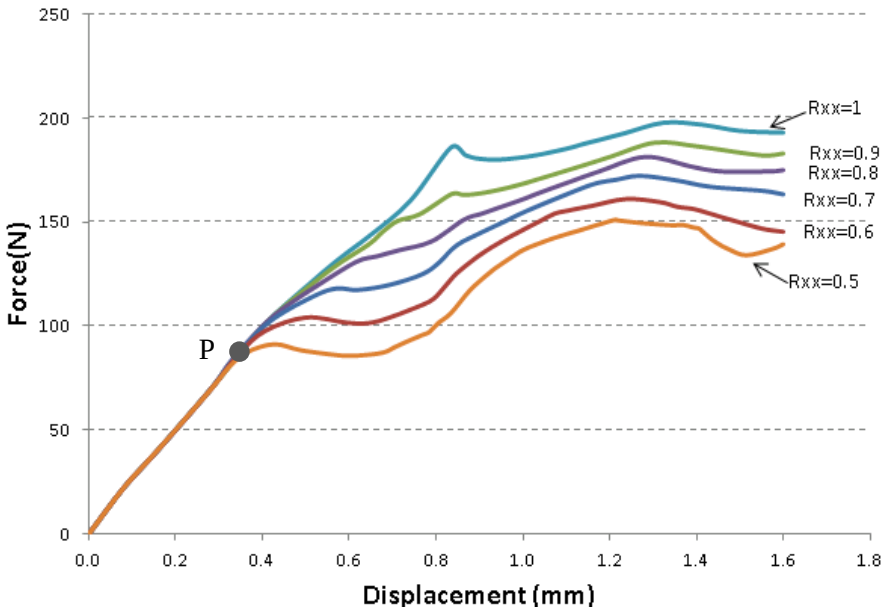

Figure 3.6 The force-displacement curves with different R_{xx}

g. Conclusion

In the discussions above, the effects of the 32 material constitutive parameters of the cardboard on the compressive behavior were analyzed. Four of them affect the

force-displacement curve more strongly than the other parameters. Thus, the total number of independent parameters is reduced from 32 to 4 and the four parameters are: E_{xf}, E_{tf}, G_{xzf} and R_{xx}. These parameters will be fine-tuned, and in other words, they were the variables in the optimization model (notice: the parameter identification problem of the system was represented as an optimization problem).

3.4.2 Constraint

The constraints of design variables (DVs) were made in Table 3.7 (Schwingshackl et al. 2006; Thakkar et al. 2008; Huang 2013). In ANSYS, tolerance is the acceptable variation in the DVs between loop computations to determine the convergence criterion. In this analysis, the tolerance of DV is set as default that equals 0.01 times the current value.

Table 3.7 Constraint on the optimization variables

Design Variable	Meaning	Lower limit (GPa)	Upper limit (GPa)
$\boldsymbol{E_{xf}}$	elastic modulus in x-direction	0.5	6
$\boldsymbol{G_{xzf}}$	Shear modulus in xz plane	0.003	0.01
$\boldsymbol{E_{tf}}$	Tangent modulus of core	0.001	0.05
$\boldsymbol{R_{xx}}$	yield stress ratio in x-direction	0.9	1

3.4.3 Objective variables (OVs)

The objective variable is the variable in the optimization, which needs to be minimized. In the problem the present work was concerned, the objective variable was the least-square deviation between the calculated and measured force-displacement, that is:

$$\text{OBJ= } \varepsilon(Q) = \frac{1}{n}\sum_{i=1}^{n}\left(\frac{F^{sim}(U_i,Q)-F^{exp}(U_i)}{F^{exp}(U_i)}\right)^2 \tag{3.18}$$

where n is the number of force-displacement points adopted in the calculated and measured curve. F^{sim} means the calculated force and F^{exp} is the measured force; U_i represents the displacement of the ith point. Q is the design variable set.

3.4.4 Optimization method

In ANSYS, two optimization methods are available: the sub-problem approximation method and the first order method. The sub-problem approximation method applies a zero-order algorithm that only requires the values of the dependent variables rather than their derivatives, which is generally capable of dealing with most of the engineering problems. The first order method requires the information of first order derivative of the dependent variables, leading to a higher accuracy but a higher computational cost. In this thesis, the sub-problem approximation method was chosen. ANSYS offers a number of optimization tools such as single-loop analysis, random, sweep, factorial and gradient tools as well. In this case, the Sweep tool analyses each design variable (DV)'s sensitivity to the objective function in the global design space. In this analysis, the sweep tool actually scans the design space, so it gets the information of the objective function over the domain. By examining this information, one can identify the one that is the smallest value of the objective function, which corresponds to the optimal design variable. The sub-problem approximation method and sweep tool are briefly introduced in the following.

Sub-problem approximation method

Consider that a general constrained problem is expressed as follows (ANSYS Inc. 2004):

$$\min\ f = f(x) \tag{3.19}$$

$$g_i(x) \le g_{imax} \qquad (i = 1,2,3,\dots,m_1) \tag{3.20}$$

$$h_{imin} \le h_i(x) \qquad (i = 1,2,3,\dots,m_2) \tag{3.21}$$

$$w_{imin} \le w_i(x) \le w_{imax} \qquad (i = 1,2,3,\dots,m_3) \tag{3.22}$$

where $f(x)$ is the objective function (the objective variable 'f'), $g_i(x), h_i(x)\ and\ w_i(x)$ are constraint functions.

In the sub-problem approximation method, the objective variable and the constraint variables are first replaced by (ANSYS Inc. 2004):

$$\hat{f}(x) = f(x) + error \tag{3.23}$$

$$\hat{g}(x) = g(x) + error \tag{3.24}$$

$$\hat{h}(x) = h(x) + error \tag{3.25}$$

$$\hat{w}(x) = w(x) + error \tag{3.26}$$

The constraints are converted to the unconstrained optimization problem by using a penalty function. The penalty function satisfies: if independent variables (e.g.,x, in this case) are feasible, the penalty function is zero; otherwise it is greater than zero. In this case, X, G, H, and W are defined as a penalty function for the design variable and constraint. As such, the problem becomes (ANSYS Inc. 2004):

Minimize

$$\mathrm{F}(\bar{x}, P_k) = \hat{f} + f_0 P_k \left(\sum_{i=1}^{n} X(x_i) + \sum_{i=1}^{m_1} G(\hat{g}_i) + \sum_{i=1}^{m_2} H(\hat{h}_i) + \sum_{i=1}^{m_3} W(\hat{w}_i) \right) \tag{3.27}$$

where f_0 is the reference objective function value used to achieve consistent unit. P_k is a response surface parameter. The subscript k is the number of the iterations during the sub-problem optimization process. P_k is increased in value as k increases, that is, ($P_1 > P_2 > P_3\ etc.$) in order to obtain accurate, converged results.

Convergence: when the convergence is reached, the sub-problem approximation iteration stops. Convergence is assumed that if all the present design $f^{(j)}$, the previous design $f^{(j-1)}$ and the best design set $f^{(b)}$ are feasible design; and one of the following conditions is satisfied (ANSYS Inc. 2004).

$$\left|f^{(j)} - f^{(j-1)}\right| \leq \tau \tag{3.28}$$

$$\left|f^{(j)} - f^{(b)}\right| \leq \tau \tag{3.29}$$

$$\left|x_i^{(j)} - x_i^{(j-1)}\right| \leq \rho_i \qquad \text{(i=1,2,3,…,n)} \tag{3.30}$$

$$\left|x_i^{(j)} - x_i^{(b)}\right| \leq \rho_i \qquad \text{(i=1,2,3,…,n)} \tag{3.31}$$

where: τ is the objective function tolerance and ρ_i is the design variable tolerance. Termination will happen when either the number of sub-problem iterations or the number of sequential infeasible design sets is equal to the limit set for them.

Sweep tool

The sweep tool is used to scan global design space. Upon the sweep tool run, each DV is scanned from minimum to maximum while the remaining other DVs are fixed at the pre-set reference. A sweep execution includes $n \times N_s$ design sets, where n is the number of DVs and N_s is the number of increments of each DV. For example, an optimization problem with 4 DVs and input N_s as 10 would sweep 40 times in total. During the iteration, the *kth* DV of a given design set $m+i$ is expressed as:

$$x^{(m+i)} = x^{(r)} + (i-1)\,\Delta\, x_k \qquad (i = 1, 2, 3, \ldots, N_s) \tag{3.32}$$

where $x^{(r)}$ means the reference DV, r is the reference design set number, and Δx_k is the increment of sweep for *kth* DV.

3.4.5 Optimization Result

The maximum number of iterations was set as 25 for the ANSYS sub-problem optimization process. The optimization problem was converged after 21 iterations. The optimal design variables are listed in Table 3.8. The result of the convergence for the ANSYS sub-problem optimization process is shown in Figure 3.7.

It is noted that the improvement 21.7% is calculated with the following formula:

$$\frac{OBJ_0 - OBJ_1}{OBJ_0} \tag{3.33}$$

where OBJ_1 is the objective function in the original model. OBJ_0 is the objective function in the model after the sub-problem method is applied.

Table 3.8 The best design set obtained from the sub-problem optimization process compared with the original parameter set

Variables	$\boldsymbol{E_{xf}}$(GPa)	$\boldsymbol{G_{xzf}}$(MPa)	$\boldsymbol{E_{tf}}$(MPa)	$\boldsymbol{R_{xx}}$	OBJ	Improvement of OBJ
Parameter set in the original model	5.0	5.0	10.0	1.0	7.28	—
Best design set of sub-problem method	2.69	5.664	1.25	0.997	5.70	21.7%

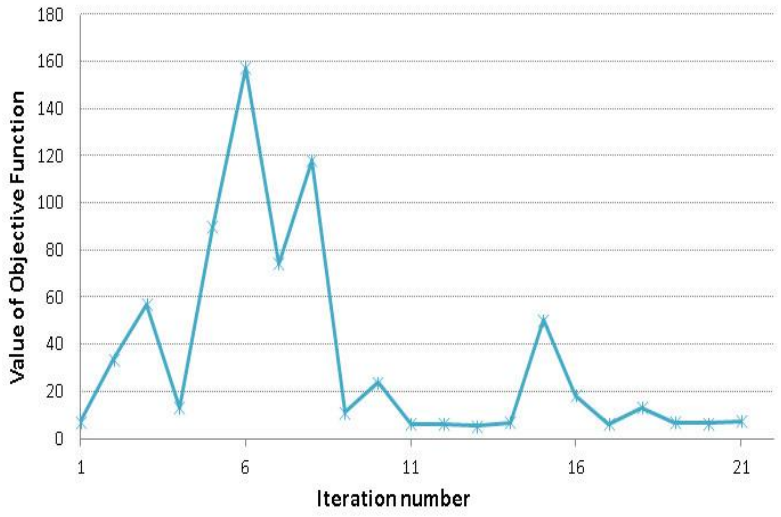

(a)

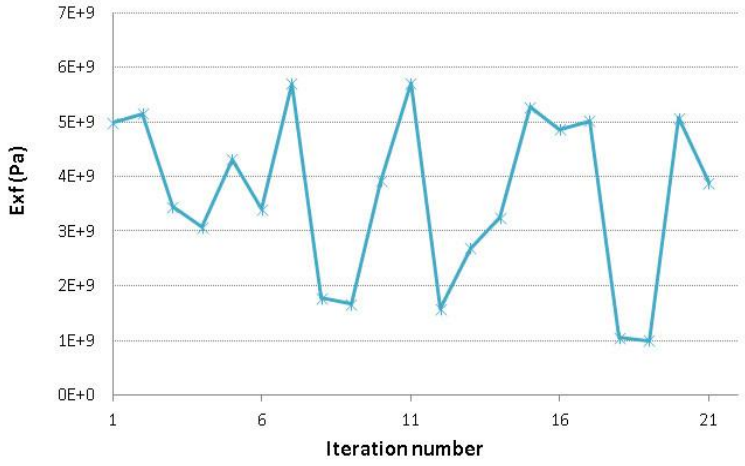
7E+9
6E+9
5E+9
4E+9
3E+9
2E+9
1E+9
0E+0
Exf (Pa)
1
6
11
16
21
Iteration number

(b)

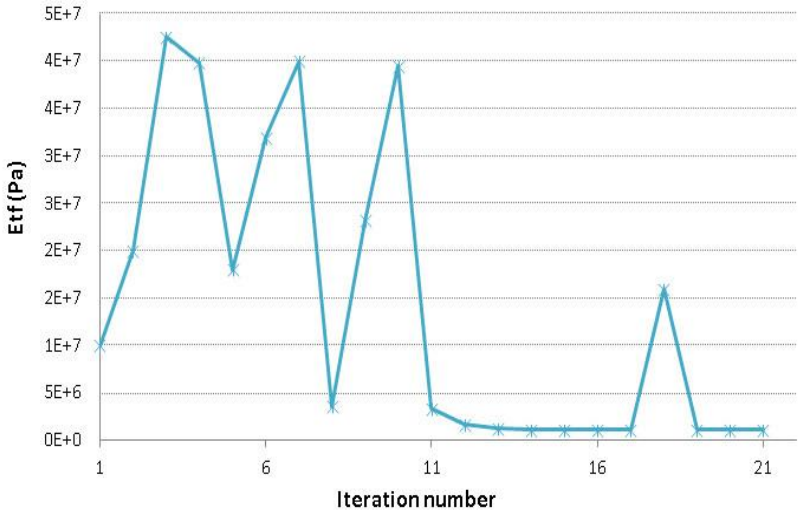
5E+7
4E+7
4E+7
3E+7
3E+7
2E+7
2E+7
1E+7
5E+6
0E+0
Etf (Pa)
1
6
11
16
21
Iteration number

(c)

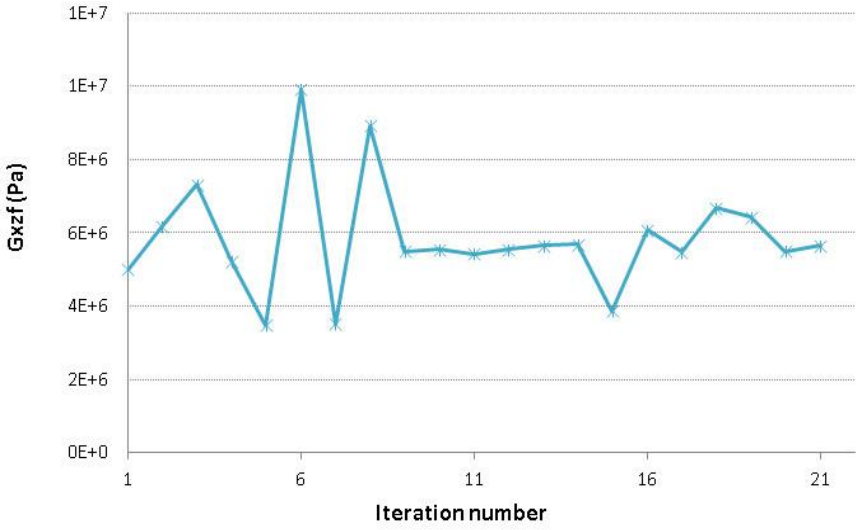
1E+7
1E+7
8E+6
6E+6
4E+6
2E+6
0E+0
Gxzf (Pa)
1
6
11
16
21
Iteration number

(d)

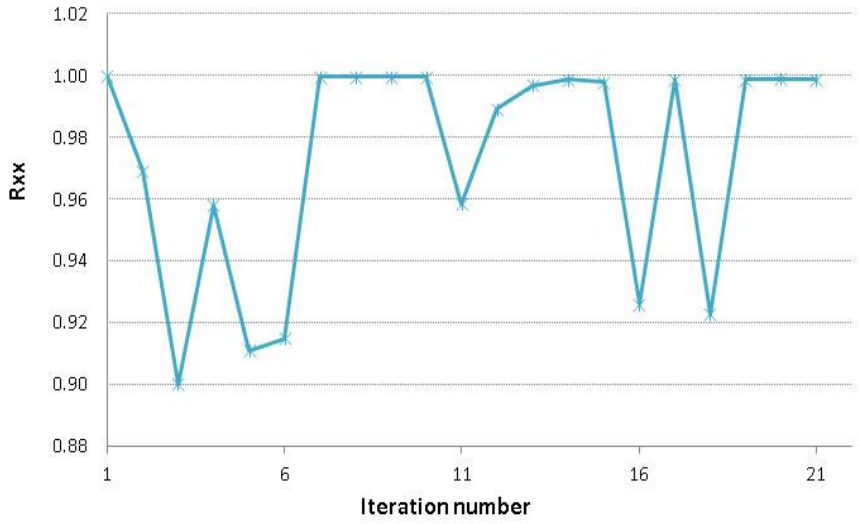

(e)

Figure 3.7 convergence behaviors of (a) objective function; (b) E_{xf};(c) G_{xzf}; (d) E_{tf}; (e) R_{xx}

Further, the sweep tool in ANSYS was applied to the optimized design obtained by the sub-problem optimization method. The number of increments of each DV: N_s= 10, namely, the sweep execution takes $4 \times 10 = 40$ times for 4 design variables in total. After the sweep analysis, a new optimal result for the objective variable was obtained and is shown in Table 3.8. It is noted that the improvement is now 31.9% compared to 21.7% based on Equation (3.33). Therefore, the results after the sweep tool are much better than that after the approximate optimization method. Figure 3.8 shows the result of sensitivity analysis of the four design variables, which gives a further assurance of the effectiveness of the choice of the four constitutive parameters.

Table 3.9 The best design set obtained from the sweep analysis compared with the original parameter set

Variables	$\mathbf{E_{xf}}$(GPa)	$\mathbf{G_{xzf}}$(MPa)	$\mathbf{E_{tf}}$(MPa)	$\mathbf{R_{xx}}$	OBJ	Improvement of OBJ
Parameter set in the original model	5.0	5.0	10.0	1.0	7.28	—
Best design set of sweep method	2.69	5.33	1.25	0.997	4.96	31.9%

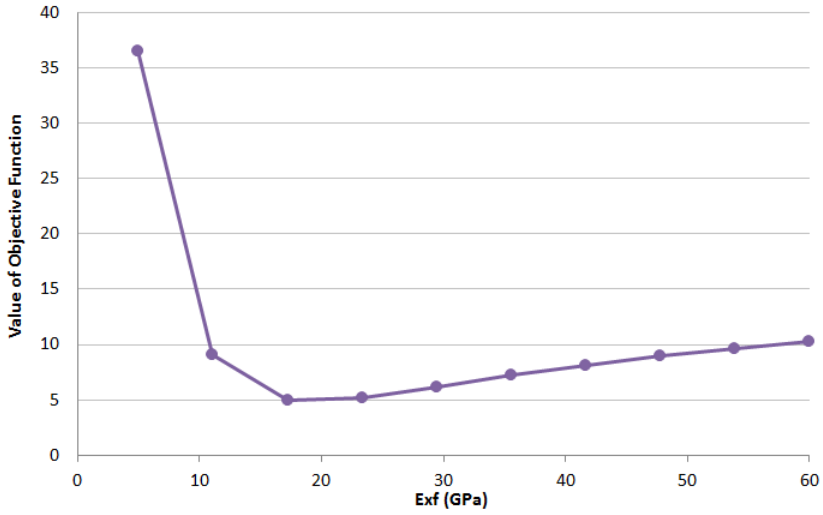
Value of Objective Function
Exf (GPa)
0
5
10
15
20
25
30
35
40
0
10
20
30
40
50
60

(a)

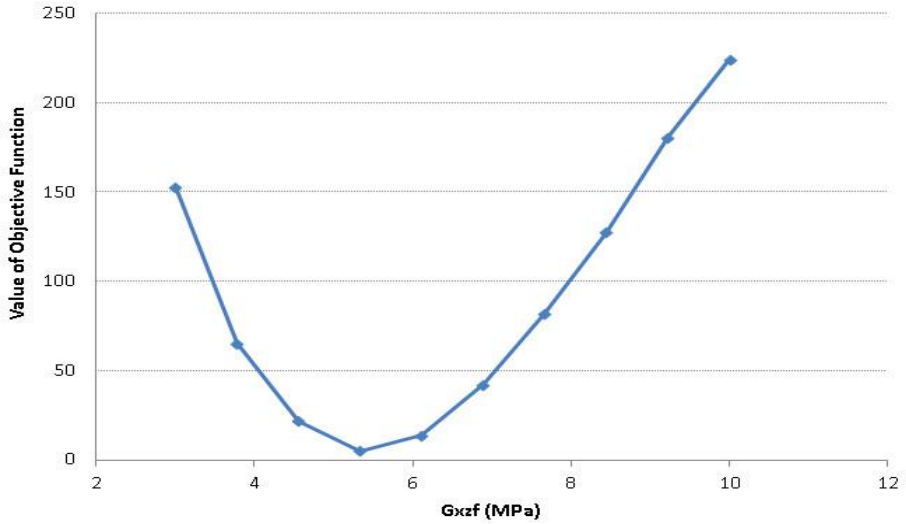
Value of Objective Function
Gxzf (MPa)
0
50
100
150
200
250
2
4
6
8
10
12

(b)

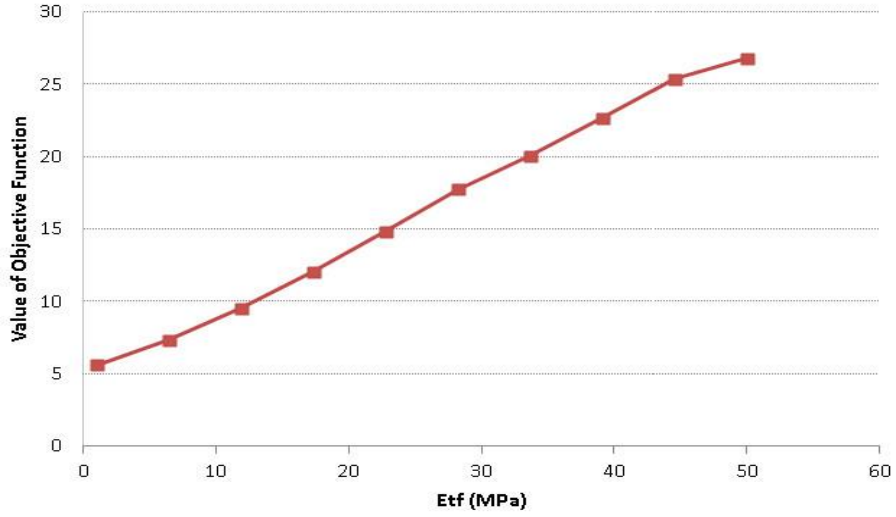
Value of Objective Function
Etf (MPa)
0
5
10
15
20
25
30
0
10
20
30
40
50
60

(c)

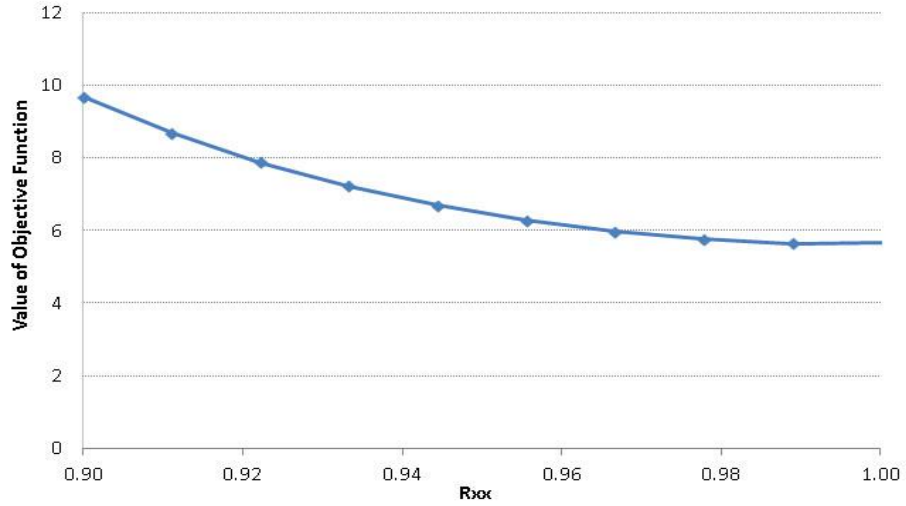

(d)

Figure 3.8 Objective function results of sweep iterations for each design variable (a) E_{xf}; (b) G_{xzf}; (c) E_{tf}; (d) R_{xx}

3.5 Results and discussion

For the sake of reducing the computational cost, a coarse analysis of the sensitivities of the constitutive parameters to the force-displacement result was first conducted, which reveals that four parameters are significant such that they were considered for fine tuning. The absolute value of the sensitivities of the four paramemters are 2.95(E_{xf}), 3e4(G_{xzf}), 8.8e2(E_{tf}) and 88.6 (R_{xx}), respectively. After applying the zero-order optimization method and the sweep tool on the FE model to the four parameters, the accuracy of the model was shown to improve by 31.9% and in particular, the model accuracy is from 7.28 to 4.96 prediction error, calculated by Equation (3.18). The sensitivity analysis to the four resulting parameters revealed that the four parameters did have significant effects on the force-displacement curve. Particularly, the average absolute value of their sensitivities to the objective function (i.e., finite points on the force-displacement curve which represent a similar meaning of sensitivity for those paramters to this curve with ultimate force but describe more accurately) are 4.77(E_{xf}), 1.02e4(G_{xzf}), 4.33e2(E_{tf}) and 50.4(R_{xx}), calcuated by Equation (3.18).

3.6 Conclusion

The constitutive parameters were analyzed to result in four parameters that have significant influence on the compressive behaviour of the cardboard. These parameters were then fine-tuned by an optimization procedure. The optimization procedure included a zero-order optimization algorithm and a sweep tool. After the optimization procedure, the convergent results were achieved, and the fine-tuned parameters were obtained. As a result, the accuracy of the model has been improved by 31.9%. The following conclusions can be drawn from the study.

First, the optimization method combined with the sub-problem method and the sweep tool is reliable and effective to the present problem.

Second, the procedure to remove the constitutive parameters that are of no significant influence on the force-displacement behavior is effective. Although the analysis seems to be coarse and ad-hoc, the subsequent optimization seems to off-set the ad-hoc analysis.

CHAPTER 4 MANUFACTURING IMPERFECTION ANALYSIS OF CORRUGATED CARDBOARDS

4.1 Introduction

Manufacturing of corrugated cardboards usually introduce some significant geometric imperfections. The materials of the cardboards are soft materials, and the control of their geometry in manufacturing is difficult. Understanding of the robustness of the model with respect to these imperfections is thus important. Imperfections on the geometry of the cardboard will introduce the non-symmetric situation in particular, and this will then induce the friction effect in the interface between the cardboard and the equipment that is placed on the top of the cardboard. The non-symmetric situation along with the friction will introduce the transversal movement (Figure 4.1), and this phenomenon was also observed by Sven (2006). The objective of this chapter is to show the effect of this particular manufacturing imperfection and its transversal movement. Section 4.2 presents the FEM model of the cardboard system with consideration of the transversal movement and compares the model predicted result with the experimental result of Huang (2013).

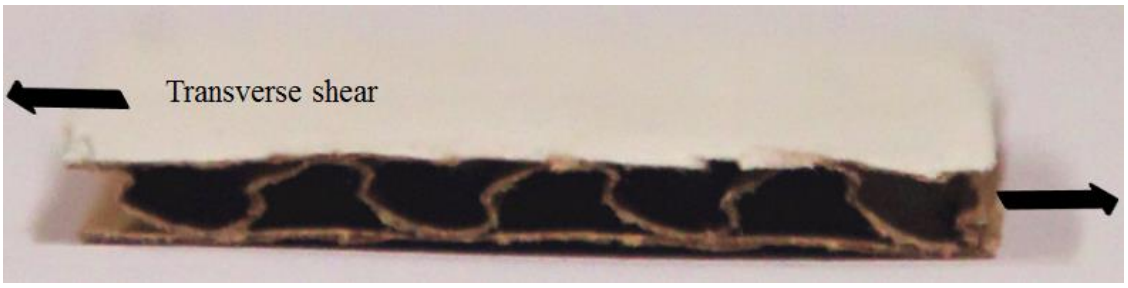

Figure 4.1 A compressed cardboard sample with transverse shear deformation

4.2 The Modified FEM Model of the Cardboard

First, the boundary condition that considers the transversal movement is shown in Figure 4.2, where the movement in the transversal direction is allowed. As such, each node on the upper liner of the cardboard has 3 DOF: two translations and one orientation, while each node on the bottom linear is completely constrained (i.e., with the 0 DOF).

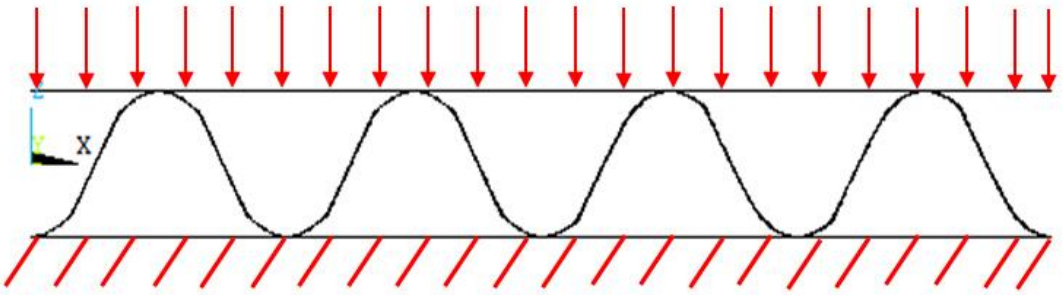

Figure 4.2 Free-edge boundary conditions

The shell element was employed to the four-flute model, which is with the same size as the experimental sample of Huang (2013), with a deflection in the x-direction on the third flute was created in the model (Figure 4.3). The deflection was made by moving a key-point in the middle height of the third flute at coordinates $x_0 = \frac{\lambda}{4}, y_0 = \frac{H}{2}$ (Point A in Figure 4.3) by an amount ξ in the x-direction, which is the same idea as Lu et al. (2001). Figure 4.3 represents the method of adding the shape imperfection. The mesh was taken the same as the one described in Section 3.2.

Figure 4.4 shows the result calculated with the model for the different transversal movements and the experimental result for the purpose of the comparison. From Figure 4.4, it can be seen that the imperfection of the flute significantly affects the plastic behaviour of the cardboard, especially the yield point. The yield points for the perfect flute, small deflection flute ($\xi = 1\%$) and the large deflected flute ($\xi = 5\%$) are 185.3Mpa, 174.9Mpa and 148.0Mpa, respectively. By changing the deflection $\xi = 1\%$ to $\xi = 5\%$, the yield strength of the cardboard model decreases, which was under the expectation. After the yield point, the trend

of the force-displacement curves with the different deflections is similar with particularly being such that the force goes downward (notice: the force goes upward when the transversal deflection is not considered in the FE model). This trend is in agreement with that observed in the experiment.

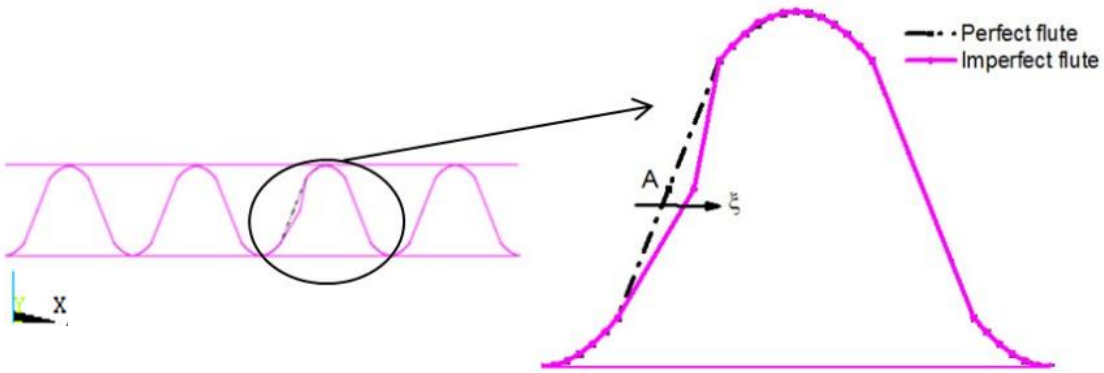

Figure 4.3 Geometry of the cross section with the imperfect flute

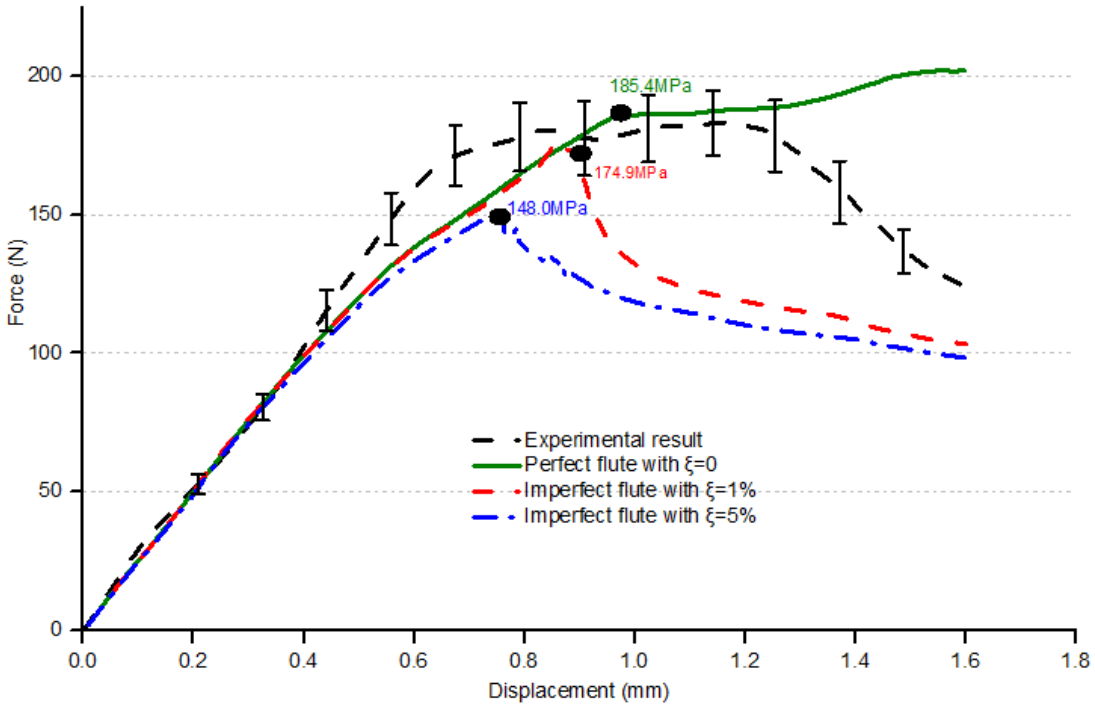

Figure 4.4 Force-displacement curves of the FE models of corrugated cardboard with perfect flute and imperfect flutes

The decreased yield strength in the imperfect model may be due to the buckling, further caused by the 2D transverse deflection. In the imperfect-flute model with the 5% deflection,

several shapes of the cross-section of the cardboard during the compression process are shown in Figure 4.5. From By examining Figure 4.4 and Figure 4.5 together, one can find the cause to support the buckling mechanism for the decrease of the yield strength of the cardboard with imperfections. First, from Figure 4.4 it can be seen that the deformation in the x-direction occurs suddenly at the displacement of 0.76 mm. Second, from Figure 4.5, the shape of the cross section of the cardboard does show a buckling form at the deformation of 0.76 mm.

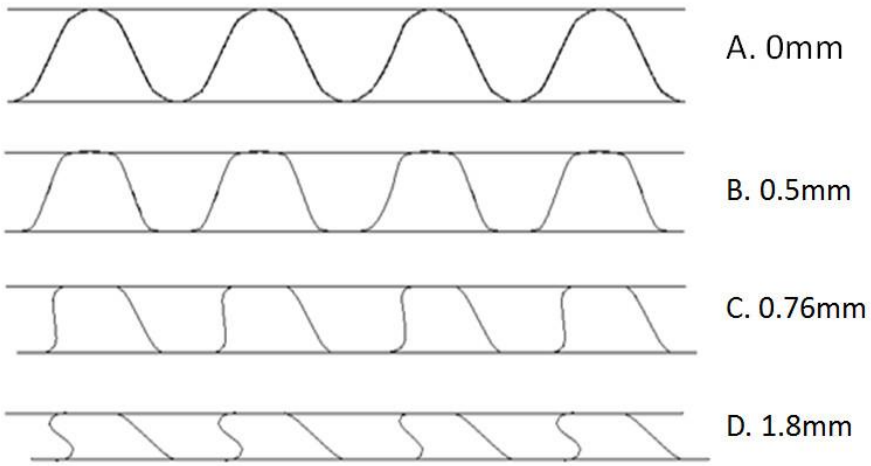

Figure 4.5 Typical deformed shape during compression calculation on imperfect-flute model (5% deflection)

4.3 Modeling of Friction between the Cardboard and Equipment

It is noted that when the cardboard is in operation, there will be an equipment or machine on the top of it and the cardboard serves as a vibration isolator. There may then be a friction between the equipment and the cardboard on their contact surface. That friction may be significant to the behavior of the cardboard and performance of the vibration isolation with the cardboard. In the following, the study of this friction is presented.

To model this friction with FEM, an isotropic plate is created and placed over the cardboard. The plate is larger than the liner of the cardboard to leave a sufficient room for the plate to slide along the top surface of the cardboard (Figure 4.6). It is noted that the testing situation

met this condition, where the test head is larger than the cardboard. This implies that the testing system and modeling system agreed on this aspect.

The test head was made of steel and it has the Young's modulus of 200 GPa and Poison's ratio of 0.3. In the finite element modeling, the boundary condition was set the same as the ones for the consideration of the imperfections with the cardboard system particularly the all the boundaries were constrained except that the boundary on the upper liner has 6 DOF (Figure 4.6).

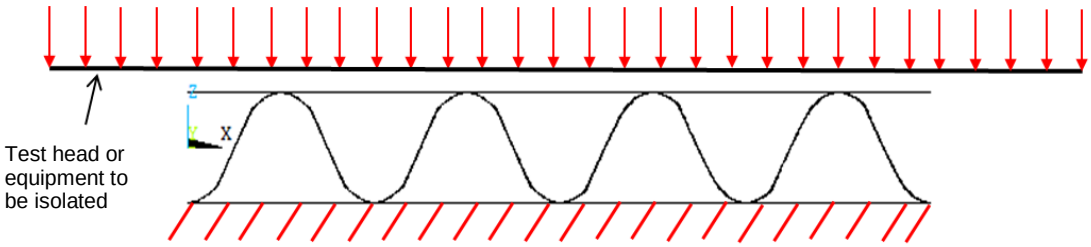

Figure 4.6 Boundary conditions with the cardboard system under the compression and subject to sliding between the top surface of the linear and the test head or equipment to be isolated

There are several kinds of contacts in terms of the friction applied in ANSYS: frictional, rough, frictionless, no separation and bounded. These are different for the frictional characteristics when the contact surfaces have or tend to have a relative movement. Frictional contact was selected since this behavior can simulate the contact with different friction coefficients (the friction coefficients between the test head and the liner in this case). The friction coefficient was set based on the Coulomb friction model. In ANSYS, The Coulomb friction model defines an equivalent shear stressτ, which decides when the two surfaces slide relative to each other. τ is described as (ANSYS Inc. 2004):

$$\tau = \mu P + COHE \qquad (4.1)$$

in which μ is the static friction coefficient; P is the contact pressure and COHE is the cohesive force. Since the cohesive force is small for the non-granular materials such as metals, paper, the cohesive force (COHE) is set to zero in this case (Vermeer et al. 2004). In

the model of cardboards, the friction coefficient μ takes several possible values to test the frictional effect on the stiffness behavior.

FE results of models with different friction conditions

After 1.2mm vertical compression, the typical contour of the contact friction stress of the FE model is shown in Figure 4.7.

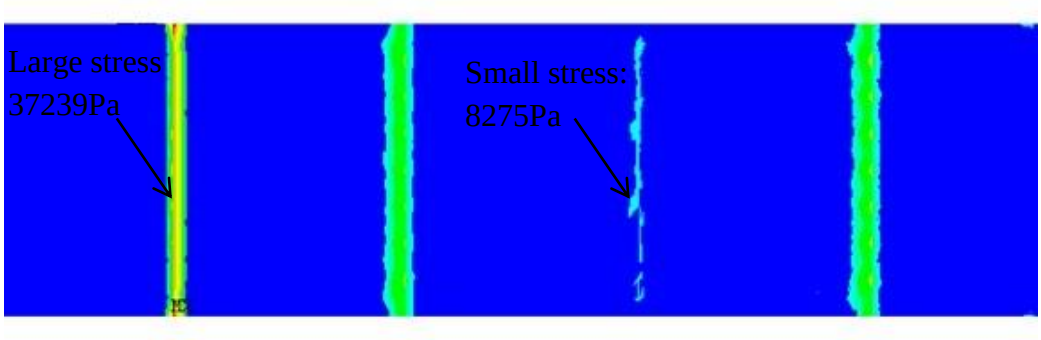

Figure 4.7 Contour of the contact friction stress between the upper liner and the upper platen

The contour of the contact friction stress implies that the static friction between the liner and the platen occurs at the position where the peaks of the flutes contact with the liner. In the four large-stress strip-like areas as showing in picture, the one closer to the imperfect position has less contact stress (8275 Pa). The left-most area furthest away from the imperfect position subjects the largest contact friction stress that is 37239 Pa.

By changing the friction coefficient μ in the range of 0.01 to 1 with an increment of 0.01 including the two extreme conditions (0.001, infinite large which corresponds to the rough surface situation in ANSYS), the force-displacement results are shown in Figure 4.8. From Figure 4.8 it can be found that when the friction coefficient is less than 0.02, the cardboard slides with respect to the test head along the transversal direction, as the force-deformation curves go down rapidly after reaching the yield point (notice the curves of Figure 4.4 where the transversal sliding occurs around the same feature). To the contrary, the curves with the friction coefficient equals to or greater than 0.03 continue to rise steadily after reaching the yield point.

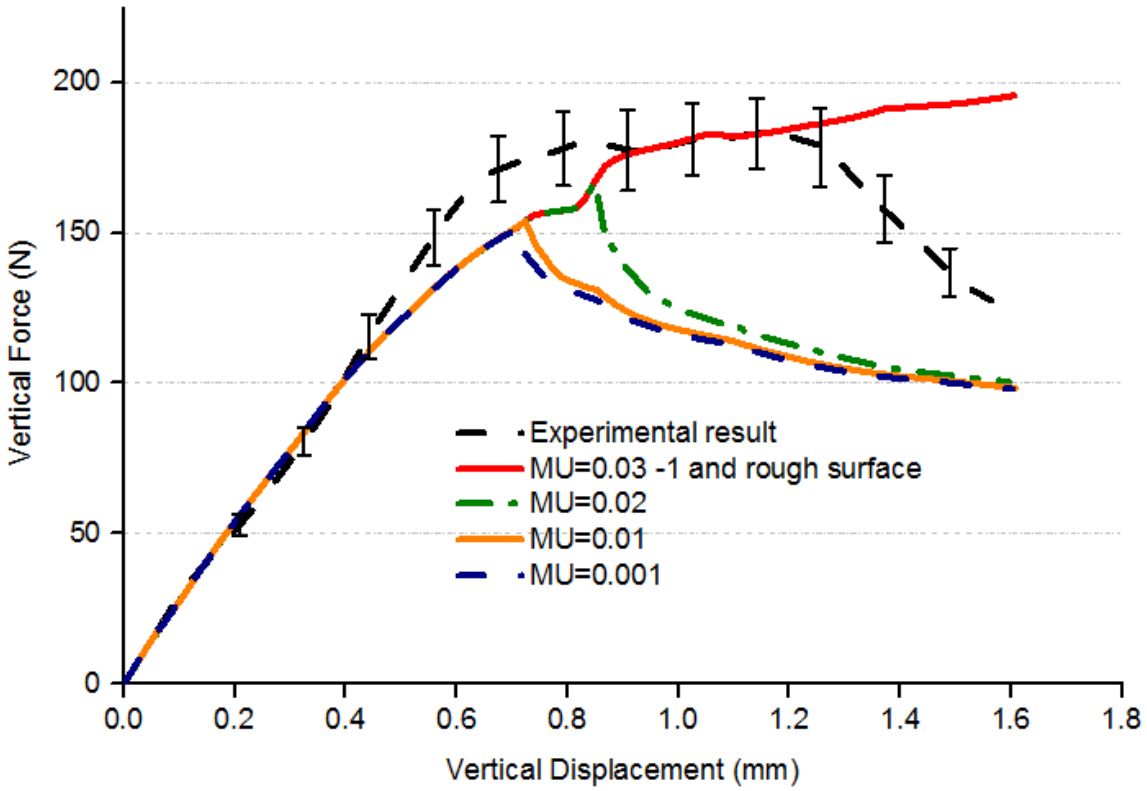

Figure 4.8 Calculations with different friction coefficients

4.4 Conclusions

This chapter discussed the effect of the geometrical imperfection of the corrugated cardboard on the force-deformation relation. Closely related to this, the chapter also discussed the effect of the friction between the cardboard and the test head. The methodology for studying the two problems was based on modeling and simulation together with limited experimental data. The experimental data was about the measured force-deformation relation for one sample. In particular, the problem of geometrical imperfection was studied by assuming that there was a transversal movement on the cardboard, that is, the different geometrical imperfections correspond to different transversal movements. As such, by assigning a different transversal movement on a node of the finite element on the profile of the flute (in the middle of the profile), a different force-deformation relation can be obtained. The problem of friction was studied by considering there is a test head or platen on the cardboard, and accordingly there is a friction between the platen and the cardboard. The finite element model incorporating this friction was developed, and the force-deformation relation with different friction coefficients

can then be found. There was also a hypothesis that the effect of the transversal movement caused by the geometrical imperfection is also related to the friction between the cardboard and platen.

The study concluded the following: (1) both the geometric imperfection and the friction between the cardboard and the platen are important factors to the force-deformation relation (compression direction), (2) the two factors are coupled, and (3) the effect of them may greatly reduce the post-yield stiffness or the so-called flow stress of the cardboard.

CHAPTER 5 MODELING OF THE DAMPING IN CORRUGATED CARDBOARDS

5.1 Introduction

Damping is an important property of the cardboard when it is used for vibration isolation. The previous work in our group did not model the damping of the cardboard instead measured the damping (Huang 2013). The model of the damping is useful to design a vibration isolator more accurately. In this chapter, modeling of the damping property of the cardboard system particularly of a serial configuration is discussed. Section 5.2 will introduce the Rayleigh damping method for modeling the damping. Section 5.3 will present the Rayleigh model of the damping for the cardboard system. In Section 5.4, the verification of the model will be discussed. A conclusion appears in the last section.

5.2 The Rayleigh Damping Model

The Rayleigh model of damping or simply called Rayleigh damping is the most popular approach to represent the damping property or behavior of a system. Rayleigh damping assumes that the damping is a linear combination of the mass and stiffness. For a general multi-DOF system, Rayleigh damping can be expressed by

$$[C] = \alpha[M] + \beta[K] \tag{5.1}$$

in which [C]=damping matrix; [M]= mass matrix; [K]=stiffness matrix; α and β are the Rayleigh damping coefficients. Considering the cardboard system as a 1 DOF system, by the orthogonal transformation, the following equation can be obtained (Chen 2013).

$$2\zeta\omega = \alpha + \beta\omega^2 \tag{5.2}$$

As such,

$$\zeta = \frac{\alpha}{2\omega} + \frac{\beta\omega}{2} \tag{5.3}$$

where ω is the natural frequency; ζ is the damping ratio. To find the Rayleigh damping coefficients α and β, one has to get at least two sets of values, namely (ζ_1, ω_1), (ζ_2, ω_2). The subscripts 1 and 2 represent the first and second modes of vibration. As such, the following equations find α and β (Chen 2013).

$$\beta = \frac{2\zeta_1\omega_1 - 2\zeta_2\omega_2}{\omega_1^2 - \omega_2^2} \tag{5.4}$$

$$\alpha = 2\zeta_1\omega_1 - \beta\omega_1^2 \tag{5.5}$$

5.3 Test-bed for determining ζ and ω

The method to determine ζ and ω was based on the literature (Mallik et al. 1999). The test-bed set-up by Huang (2013) was re-used in this thesis (Figure 5.1). A cardboard with the length 60.8 mm, width 38 mm was taken as a specimen, and load 1.94 kg was applied to the specimen. Two accelerometers were placed on the top of the steel block and of the vibration exciter, respectively (Figure 5.1b). The excitation was generated and controlled by the schematic diagram of the test-bed, as shown in Figure 5.2.

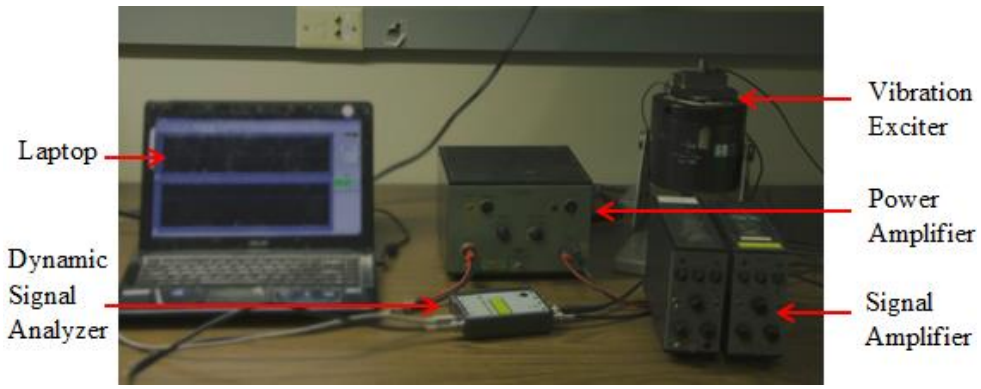

(a)

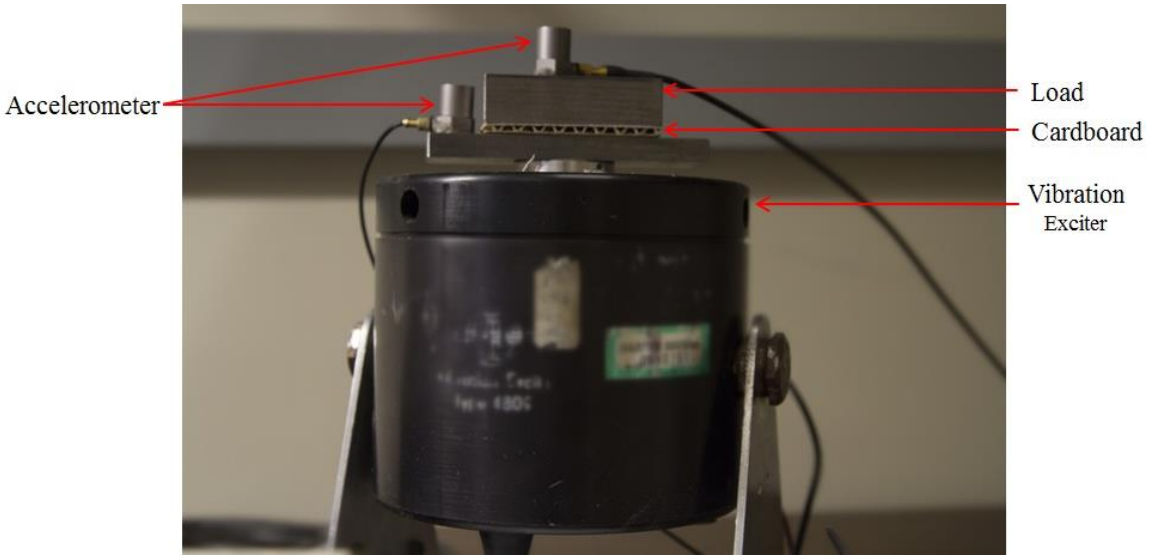

(b)

Figure 5.1 (a) Test-bed for damping measurement of the cardboard (b) Vibration exciter

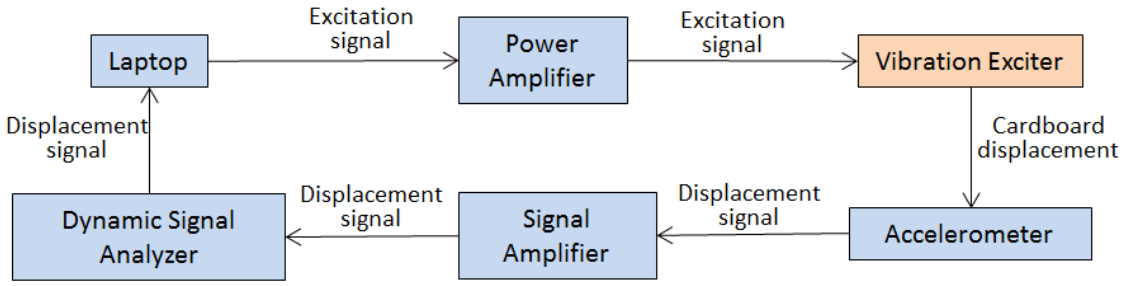

Figure 5.2 Function diagram of the test-bed

The acceleration sensors measure the displacements (A_{in}) at the top of the exciter and that (A_{out}) at the top of the cardboard. The ratio of A_{out} to A_{in} is called transmissibility (Mallik et al. 1999; Huang 2013) and the ratio can then be calculated by

$$T_r = \left|\frac{A_{out}}{A_{in}}\right| = \sqrt{\frac{1 + (2\zeta\lambda)^2}{(1-\lambda^2)^2 + (2\zeta\lambda)^2}} \tag{5.6}$$

where $\lambda =$ Frequency ratio, $\zeta =$ damping ratio, A_{out} means the energy out of system and A_{in} represents the energy into system.

When λ=1 (i.e., in a resonance state), the damping ratio can be found by

$$\zeta = \frac{1}{2}\sqrt{\frac{1}{T_r^2 - 1}} \tag{5.7}$$

Figure 5.3 shows the result of the relation between the transmissibility and the frequency. From this figure, the transmissibility and frequency can be read, which are (8.06, 60 Hz) and (10.79, 110Hz), respectively.

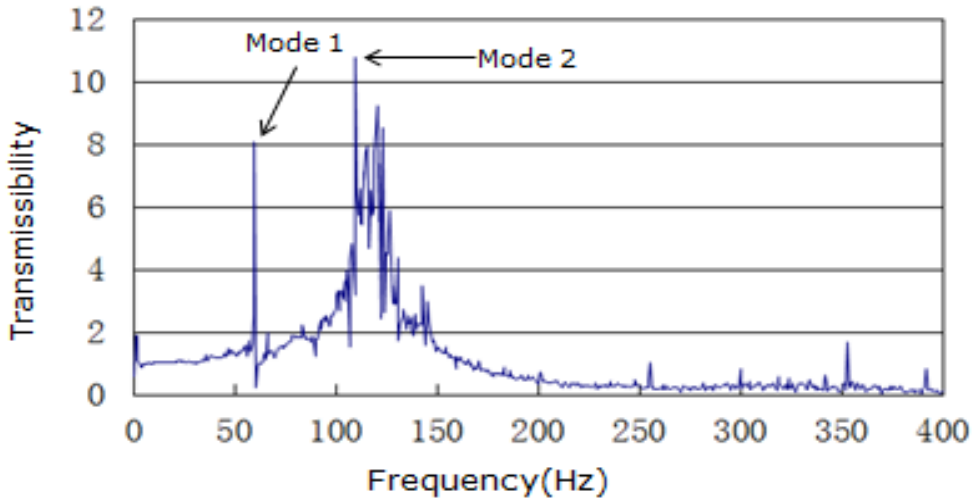

Figure 5.3 Typical result of the transmissibility vs frequency

As such, the damping ratios were found to be 0.0625 in mode one and 0.0465 in mode two. Now, two sets of the damping ratio and natural frequency are (0.0625, 60 Hz), (0.0465, 110 Hz), respectively. Subsequently, the Rayleigh damping coefficients were calculated from Equation (5.4) and Equation (5.5), respectively, and those were: $\alpha = 4.850000$, $\beta = 0.000736$. Therefore, the Rayleigh damping matrix [C] of the cardboard was obtained as follows:

$$[C] = 4.850000[M] + 0.000736[K] \tag{5.8}$$

5.4 Verification of the Damping Model

The verification of the damping model of the corrugated cardboard was carried out by means of the test-bed, as built by Huang (2013). The schematic diagram of the test-bed is shown in Figure 5.4a, and the schematic diagram of the signal flow is shown in Figure 5.4b. Furthermore, a comparison of the model prediction and the experimental measurement was made at the point of time when the resonance occurs. This is so because in the resonance situation, the role of damping is at its maximum.

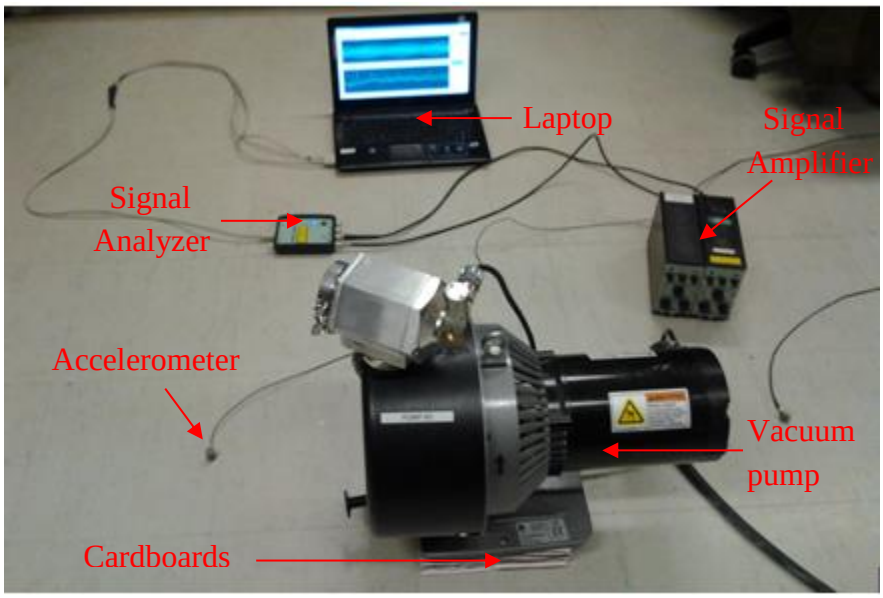

(a)

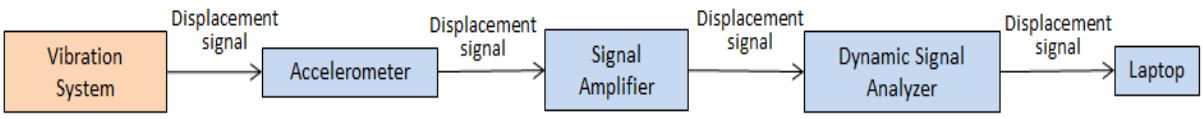

(b)

Figure 5.4 (a) the test-bed for displacement measurement in the pump-cardboard-ground vibration system (Huang 2013) (b) the signal flow of the test.

Further, a comparison was made for both the damping coefficient, measured by Huang (2013), and the one, proposed in this thesis, based on the Rayleigh damping model. The

comparison was made for the transmissibility (T_r), which was defined as the ratio of the force (F_T) transmitted to the ground through the cardboard to the force generated by the pump (F_0). The transmissibility can be further expressed based on the definition of F_T and F_0 by the stiffness, damping and frequency, which is given by

$$\mathrm{T_r} = \frac{F_T}{F_0} = \left\{\frac{\mathrm{k}^2 + \omega^2\mathrm{c}^2}{(\mathrm{k} - \mathrm{m}\omega^2)^2 + \omega^2\mathrm{c}^2}\right\}^{1/2} \tag{5.9}$$

where ω is the operating frequency of the pump, m is the mass of the pump, and c is the damping of the isolator, and k is the stiffness of the isolator.

5.4.1 Layer of the cardboard system at the resonance frequency

The cardboard system considered in this thesis was a set of cardboards that connected in serial. It was further assumed that these cardboards are identical. Therefore, there is ($c_0 = c_1 = \cdots = c_{n-1}$). The total or equivalent damping (c_{eqv}) of the cardboard system is given by (Rao and Horton 2003)

$$c_{eqv} = \frac{c_0}{n} \tag{5.10}$$

Likewise, with the same stiffness ($k_0 = k_1 = \cdots = k_{n-1}$), the total or equivalent stiffness (k_{eqv}) of the system is expressed by (Rao and Horton 2003)

$$\mathrm{k_{eqv}} = \frac{\mathrm{k_0}}{\mathrm{n}} \tag{5.11}$$

Let the exciting frequency ω is equal to the natural frequency of the system ω_n. This then gives:

$$\omega = \omega_\mathrm{n} = 183.69\ \mathrm{rad/s} \tag{5.12}$$

Note that the pump has a high rotational speed of 183.69rad/s (Pump manual, 2010). Further, there is the following calculation about the stiffness, namely

$\omega_n = \sqrt{\frac{k_n}{m}}$ (Rao, 2003) and thus,

$$\mathrm{k_n} = \omega_\mathrm{n}^2 \mathrm{m} = 183.69^2 \times 34 = 1147229\ \mathrm{N/m} \tag{5.13}$$

Note that the stiffness of one piece of the cardboard k_0 in this experiment was 7110000N/m, which is 6.19 times of the stiffness in resonance, i.e., based on Equation (5.11), the number of layer n is:

$$\mathrm{n} = \frac{\mathrm{k_0}}{\mathrm{k_n}} = 6.19 \approx 6 \tag{5.14}$$

5.4.2 Vibration Test

The vibration test employed the method in Huang's thesis (Huang 2013). Both accelerations with cardboards (a_{with}) and without cardboards ($a_{without}$) were measured and recorded. In the Huang's test, a 6-layer-cardboard system was connected in serial (Figure 5.4) and each cardboard is 158 mm long, 210 mm wide. The transmissibility ratio T_r was given by (Huang 2013)

$$T_r = \frac{F_T}{F_0} = \frac{m_{ground} \times a_{with}}{m_{ground} \times a_{without}} = \frac{a_{with}}{a_{without}} \tag{5.15}$$

where, F_T is the magnitude of the output force on the ground; F_0 is the magnitude of the input force from the pump; m_{ground} is the mass of the ground; a_{with} is the acceleration on the ground with the cardboards; $a_{without}$ is the acceleration on the ground without the cardboards ($a_{without}$).

The typical measured accelerations on the ground with and without the 6-layer cardboards are plotted in Figure 5.5.

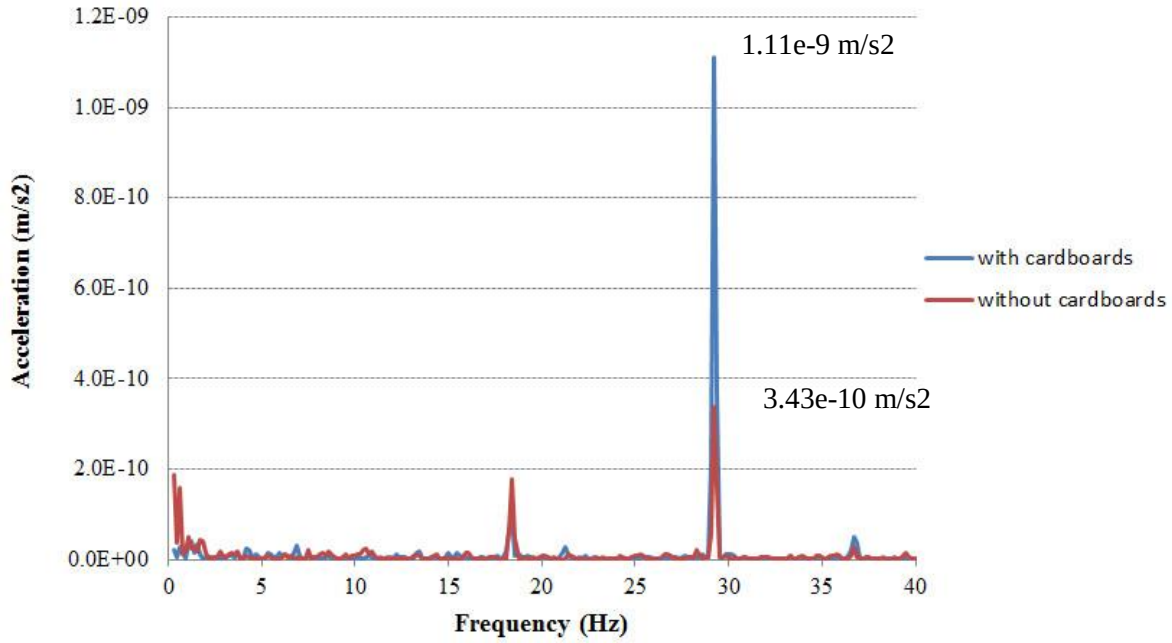

Figure 5.5 Measurement results

In this test, only the acceleration at the frequency of 29.25 Hz (183.69 rad/s) was measured as the frequency was the operation frequency of the pump. The measured accelerations transmitted from the pump with and without cardboards to the ground at 29.25 Hz are $1.11 \times 10^{-9}\ \mathrm{m/s^2}$ and $3.43 \times 10^{-10}\ \mathrm{m/s^2}$, respectively.

Thus, based on Equation (5.15), the transmissibility of the 6-layer cardboards is

$$\mathrm{T_r} = \frac{1.11 \times 10^{-9}}{3.43 \times 10^{-10}} = 3.24 \qquad (5.16)$$

By repeating the measurements, the mean transmissibility

$$\mathrm{T_r} = 3.28$$

5.4.3 Comparison

In Huang's work, the damping of the system with 1-layer cardboard was $861\ \mathrm{Ns/m}$. Based on Equation (5.10), the damping (c) of the 6-layer cardboard system is $143.5\ \mathrm{Ns/m}$. Likewise, the stiffness of the system with 1-layer cardboard is 7110000 N/m. Based on Equation (5.11), the stiffness (k) of the 6-layer cardboard system is 1185000 N/m. The

mass $m = 34kg$ and the frequency $\omega = 183.69\ rad/s$ (Pump manual, 2010). Substituting the values of c, k, m and ω into Equation (5.9) yields to:

$$T_r = \left\{ \frac{1185000^2 + 183.69^2 \times 143.5^2}{(1185000 - 34 \times 183.69^2)^2 + 183.69^2 \times 143.5^2} \right\}^{1/2} = 25.73 \qquad (5.17)$$

The Rayleigh damping model of the cardboards is obtained in Equation (5.8). Substituting the same stiffness and the same mass as that in Huang's model into Equation (5.8) leads to:

$$c = 1036.6\ Ns/m \qquad (5.18)$$

Thus, the transmissibility calculated by using the Rayleigh damping is

$$T_r = \left\{ \frac{1185000^2 + 183.69^2 \times 1036.6^2}{(1185000 - 34 \times 183.69^2)^2 + 183.69^2 \times 1036.6^2} \right\}^{1/2} = 6.18 \qquad (5.19)$$

The transmissibility calculated using the damping in Huang's work has an error of 87%, while the transmissibility calculated by the Rayleigh damping developed in this thesis has the error of 47%. Therefore, the transmissibility calculated by the Rayleigh damping is more accurate.

5.5 Conclusion

In this chapter, the Rayleigh damping model was developed for the cardboards in this thesis. Two constant coefficients α and β in the Rayleigh damping were determined by the experiment. The verification was conducted by the pump-cardboard-ground vibration system. The result concluded that the Rayleigh damping is more accurate than the Huang's measurement based approach.

CHAPTER 6 CONCLUSION AND FUTURE WORK

6.1 Overview

This thesis presented a study on improving the method for calculating the stiffness and damping of the corrugated cardboard for the vibration isolation application. There are many studies on the properties of stiffness and damping and the models of them. Recently, Huang (2013) first studied the stiffness and damping of the corrugated cardboards for the vibration isolation application. However, there are some shortcomings both in Huang's and in others' as follows.

(1) The accuracy of the models for stiffness and damping is not very high. One plausible cause may be due to the difficulty to determine some constitutive parameters in the cardboard. Yet, another reason is that some physics are not taken into account in the model, e.g., the geometrical imperfection and friction between the cardboard and the equipment to be isolated.

(2) The damping of the cardboard is not modelled, which may give some inaccuracy in the design of the isolation system with the cardboards.

This thesis was motivated by overcoming the foregoing shortcomings. Particularly, the first work of the thesis was to determine the constitutive parameters more accurately by applying the system identification technique, which was described in Chapter 3. The second work of the thesis was to model the geometrical imperfection and friction between the cardboard and the equipment, which was described in Chapter 4. The third work of the thesis was to model the damping of the cardboard, which was described in Chapter 5.

The following are conclusions drawn from this thesis:

(1) The constitutive parameters are indeed very important to the accuracy of the modelling for the stiffness in the compression direction or the force-deformation relation in the vertical direction, which made FEM prediction more accurate. Accuracy of prediction increased by 31.9% after applying the parameter identification procedure compared to the accuracy of the model in Huang's thesis (Huang 2013).

(2) The geometrical imperfection of the cardboard and friction between the cardboard and equipment are very important factors to the accuracy of the modeling for the stiffness as well. Generally, less deflection of flute or greater interface friction coefficient result in a stronger yield strength of the cardboard. These two factors are coupled to affect the post-yield stiffness by giving rise to transversal movement.

(3) The Rayleigh model for the damping of the cardboard has a sufficient accuracy for the cardboard by decreasing the error from 87% to 47%. Thus, the Rayleigh damping contributes to the accuracy of the isolation system considerably.

6.2 Contributions

The main contributions of the thesis are summarized in the following:

(1) The provision of an effective procedure to determine the constitutive parameters more accurately via a system identification technique. Through a simple compression testing, these parameters were determined. This procedure can readily be applied to other similar problems.

(2) The finding that the geometrical imperfection and friction between the cardboard and equipment are coupled and these have a significant effect on the accuracy of the model for the stiffness of the cardboard.

(3) The provision of a model for the damping of the cardboard that could be used to design the isolation system of cardboards more accurately.

6.3 Future Work

There are a number of potential works worthy of further investigation. The following are some of these possible works:

First, the different optimization algorithms can be applied in the optimization of the constitutive parameters in the FE model of the corrugated cardboards, such as genetic algorithm and the first-order method. This may provide more options for identifying the material parameters based on the different requirements of accuracy and computational cost.

Second, the objective function in the optimization model in this thesis is formed based on the average values of the force and displacement in the experiment. Other features such as the stress field can be considered as the objective function.

Third, the geometrical imperfections in the out-of-plain direction and even the 3-D imperfection need to be studied more thoroughly and experimentally

Finally, the horizontal movement of the vacuum pump can be considered in the damping models.

REFERENCES

Aboura, Z., N. Talbi, S. Allaoui, and M. L. Benzeggagh. 2004. Elastic behavior of corrugated cardboard: experiments and modeling. Composite Structures 63:53–62.

Allansson, A., and B. Svärd. 2001. *Stability and collapse of corrugated board.* Unpublished M.Sc. thesis. Structural Mechanics. Lund University, Lund, Sweden.

ANSYS Inc. 2004. *Theory Reference.* Canonsburg , PA.

ANSYS Inc. 2005. *ANSYS Advanced Analysis Techniques Guide, Ansys Help.* Canonsburg, PA.

Baum, G. A., D. C. Brennan, and C. C. Habeger. 1981. Orthothopic elastic constants of paper. Tappi 64:97–101.

Biancolini, M. E. 2005. Evaluation of equivalent stiffness properties of corrugated board. Composite Structures 69:322–328.

Biancolini, M. E., and C. Brutti. 2003. Numerical and experimental investigation of the strength of corrugated board packages. Packaging Technology and Science 16:47–60.

Budynas, R. G. 1999. Advanced Strength and Applied Stress Analysis (2nd ed.). McGraw-Hill, Boston.

Carlsson, L. a., T. Nordstrand, and B. Westerlind. 2001. On the elastic stiffnesses of corrugated core sandwich. Journal of Sandwich Structures and Materials 3:253–267.

Chen, W. 2013. *Development of a kinetic model for loop-free colonoscopy technology.* Unpublished Ph.D. thesis. University of Saskatchewan, Saskatoon, SK, Canada.

Dayyani, I., S. Ziaei-Rad, and H. Salehi. 2011. Numerical and experimental investigations on mechanical behavior of composite corrugated core. Applied Composite Materials 19:705–721.

De Silva, C. W. 2006. Vibration: fundamentals and practice (2nd ed.). CRC press, Boca Raton.

Gilchrist, A. C., J. C. Suhling, and T. J. Urbanik. 1998. Nonlinear finite element modeling of corrugated board. Mechanics of Cellulosic Materials ASME 231:101–106.

Haj-Ali, R., J. Choi, B.-S. Wei, R. Popil, and M. Schaepe. 2009. Refined nonlinear finite element models for corrugated fiberboards. Composite Structures 87:321–333.

Hammou, A. D., P. T. Minh Duong, B. Abbès, M. Makhlouf, and Y.-Q. Guo. 2012. Finite-element simulation with a homogenization model and experimental study of free drop tests of corrugated cardboard packaging. Mechanics & Industry 13:175–184.

Huang, J. 2013. *Investigation of corrugated cardboard for vibration isolation.* Unpublished M.Sc. thesis. University of Saskatchewan, Saskatoon, SK, Canada.

Imaoka, S. 2000. *ANSYS tips & tricks: structure shell elements, part 1.* Redondo beach, California, USA.

Jiménez-Caballero, M. A., I. Conde, B. García, and E. Liarte. 2009. Design of different types of corrugated board packages using finite element tools. SIMULIA Customer Conference. London, UK.

Kirwan, M. J. 2012. Handbook of Paper and Paperboard Packaging Technology (2nd ed.). John Wiley & Sons, London, UK.

Krusper, A., P. Isaksson, and P. Gradin. 2008. Modeling of out-of-plane compression loading of corrugated paper board structures. Journal of Engineering Mechanics 133:1171–1177.

Lu, T. J., C. Chen, and G. Zhu. 2001. Compressive behaviour of corrugated board panels. Journal of Composite Materials 35:2098–2126.

Mallik, A. K., V. Kher, M. Puri, and H. Hatwal. 1999. On the modelling of non-linear elastomeric vibration isolators. Journal of Sound and Vibration 219:239–253.

Mann, R. W., G. A. Baum, and C. C. Habeger Jr. 1979. Determination of all nine orthotropic elastic constants for machine-made paper. Tappi 63:163–166.

Nguyen, M. Q., S. S. Jacombs, R. S. Thomson, D. Hachenberg, and M. L. Scott. 2005. Simulation of impact on sandwich structures. Composite Structures 67:217–227.

Nordstrand, T. 2003. *Basic testing and strength design of corrugated board and containers.* Unpublished Ph.D. thesis. Lund University, Lund, Sweden.

Nordstrand, T. M. 1995. Parametric study of the post-buckling strength of structural core sandwich panels. Composite Structures 30:441–451.

Nordstrand, T. M., and L. A. Carlssonb. 1997. Evaluation of transverse shear stiffness of structural core sandwich plates. Composite Structures 8223:145–153.

Patel, P., T. Nordstrand, and L. A. Carlssonb. 1997. Local buckling and collapse of corrugated board under biaxial stress. Composite Structures 39:93–110.

Pommier, J. C., J. Poustis, E. Fourcade, and P. Morlier. 1991. Determination of the critical load of a corrugated box subjected to vertical compression by finite element methods. Proceedings of the 1991 International Paper Physics Conference (pp. 437–447). Kona, HI.

Rajesh, E., and M. Sivaprakash. 2013. Analysis of friction factor by employing the ring compression test under different lubricants. International Journal of Advancements in Research & Technology 4:1163–1171.

Rao, S. S., and M. J. Horton. 2003. Mechanical Vibrations (5th ed.). Prentice Hall, Upper Saddle River.

Schwingshackl, C. W., G. S. Aglietti, and P. R. Cunningham. 2006. Determination of honeycomb material properties: existing theories and an alternative dynamic approach. Journal of Aerospace Engineering 19:177–183.

Sek, M. 2009. Dynamic Response of a Multilayer Corrugated Structure with History-Dependent Properties Subjected to Transient Loads. Proceedings of SEM 2009 Annual Conference on Experimental and Applied Mechanics (pp. 1–3). Albuquerque NM, USA.

Standard Specification for Corrugated and Solid Fiberboard Sheet Stock (Container Grade) and Cut Shapes. ASTM standard D4727. 2007.

Stenberg, N. 2003. A model for the through-thickness elastic–plastic behaviour of paper. International Journal of Solids and Structures 40:7483–7498.

Talbi, N., A. Batti, R. Ayad, and Y. Q. Guo. 2009. An analytical homogenization model for finite element modelling of corrugated cardboard. Composite Structures 88:280–289.

Thakkar, B. K., L. G. J. Gooren, R. H. J. Peerlings, and M. G. D. Geers. 2008. Experimental and numerical investigation of creasing in corrugated paperboard. Philosophical Magazine 88:3299–3310.

Twede, D., and S. E. M. Selke. 2005. Cartons, Crates and Corrugated Board: Handbook of Paper and Wood Packaging Technology. DEStech Publications, Inc, Lancaster.

Vermeer, P. A., W. Ehlers, H. J. Hermann, and E. Ramm. 2004. Modelling of Cohesive-Frictional Materials: Proceedings of Second International Symposium on Continuous and Discontinuous Modelling of Cohesive-Frictional Materials. CRC Press, Stuttgart.